Journal of Molecular Liquids 350 (2022) 118534

Contents lists available at ScienceDirect

Journal of Molecular Liquids

journal homepage: www.elsevier.com/locate/molliq

Adsorption of Cr (VI), and Pb (II) from aqueous solution by 1-Butyl-3-methylimidazolium bis(trifluoromethylsulfonyl)imide functionalized biomass Hazel Sterculia (*Sterculia Foetida* L.)

Anjani R.K. Gollakota [a,*], Venkata Subbaiah Munagapati [b], Chi-Min Shu [b,*], Jet-Chau Wen [a,b,*]

[a] Department of Safety, Health, and Environmental Engineering, National Yunlin University of Science and Technology, Douliou city, Yunlin 64002, Taiwan, ROC
[b] Research Centre for Soil & Water Resources and Natural Disaster Prevention (SWAN), National Yunlin University of Science and Technology, Douliou city, Yunlin 64002, Taiwan, ROC

ARTICLE INFO

Article history:
Received 15 November 2021
Revised 10 January 2022
Accepted 11 January 2022
Available online 13 January 2022

Keywords:
Hazel *Sterculia Foetida L*
Ionic liquid
Adsorbent
Hexavalent chromium
Divalent lead

ABSTRACT

Biomass functionalization using a green solvent (ionic liquids-IL) is a new technology for water remediation. When sorbent materials are functionalized with green solvents or ionic liquids, the load of chemical separation methods is greatly reduced and recovery of ILs is facilitated. The purpose of this study is to determine the ability of an ionic liquid activated Hazel Sterculia foetida L. (HS) seed-based sorbent to remove Cr (VI) and Pb (II) from aqueous streams under enhanced ambient conditions. When compared to the raw HS, the IL functionalization of the adsorbent significantly improved the surface characteristics, i.e., increased surface area. Subsequently, the adsorption behavior of HS-IL was examined in detail for Cr (VI) and Pb (II), taking into account the effects of pH (2–10), contact time (0–300 min), speed (100–500 rpm), starting concentrations (10–100 mg/L), and temperature (303–323 K). Additionally, the adsorption processes of Cr (VI) and Pb (II) were fully evaluated using the Langmuir, Freundlich, Sips, and Toth two-and three-parameter models. When HS + IL was compared to HS (qm = 29.2 mg/g for Cr (VI); qm = 36.4 mg/g for Pb (II), the Langmuir isotherm model predicted a maximum adsorption capacity of q_m = 82.9 mg/g (Cr(VI)); 108.63 mg/g (Pb (II)). Furthermore, kinetic modeling investigations demonstrated that the adsorption of Cr (VI), Pb (II) was better suited to a pseudo-second order model (R^2 > 0.99). Moreover, the desorbing agents HCl and NaOH recovered the adsorbent (HS, HS-IL) from Cr (VI) and Pb (II) metal solutions, respectively. Finally, the reusability of the adsorbent (HS-IL) shows promise for Pb (II) up to six cycles and three Cr (VI) cycles.

1. Introduction

Water is a demanding molecule on planet earth and a source of sustainable life. While water surrounds the majority of the globe, only about a quarter of it is potable and suitable for human use. But, the ongoing urbanization, industrialization is further depleting and straining the water bodies through the discharge of toxic organic/inorganic effluents. These inorganic contaminants originate from mining, fertilizer, batteries, pesticides, refineries, tanning, and paper industries release millions of tons of effluents comprising heavy metal ions (HMI's) Zn, Pb, Cr, Cd, As, Ni etc. [1]. These HMI's enter the food chain through groundwater causes eutrophication, thereby disturbing human, animal and marine ecologies. Specifically, Pb, Cr toxic potent metals were inevitable in ground water and upon exposure at trace minute concentrations causes kidney, liver and anemic disorder, and at higher concentrations result carcinogenic effects [2]. In flora and fauna these metals (Cr, Pb) hinder the growth of plants, disrupt the transport and disturb the process for photosynthesis. Cr exists as trivalent and hexavalent in aqueous phase, among which Cr (VI) is thermally stable than Cr (III), and tends to enter the cell wall of human, thus regarded as human carcinogen [3–5]. Whereas, Pb (II) is known as neurotoxic element, that highly affects the organ, hematopoietic system, and normal functioning of the human body.

These concerns lead to several treatment methodologies such as; co-precipitation, membrane filtration, reverse osmosis, ion-exchange, solvent extraction, chemical oxidation or reduction, phytoextraction, coagulation, adsorption, and numerous adsorbents namely; activated carbon, biomaterials, clay/layered double hydroxides, hydrogels, bio chars, zeolites, silica based materials, and nanocomposites etc. [6]. Among which adsorption, is majorly opted due to the ease of operation, cost-effectiveness, high performance, and scalability. Moreover, the viability and fidelity

* Corresponding authors.
E-mail addresses: gollakota.iitg@gmail.com (A.R.K. Gollakota), shucm@yuntech.edu.tw (C.-M. Shu), wenjc@yuntech.edu.tw (J.-C. Wen).

https://doi.org/10.1016/j.molliq.2022.118534
0167-7322/

of the bio-based materials such as algae, bagasse in adsorption of metals are extensively revealed through several research studies [7,8]. Hence, a new natural low-cost abundantly available adsorbent material Hazel *Sterculia Foetida L.,* (HS) has been introduced as an adsorbent in separating Pb, Cr ions from the aqueous solution. Further, the success of an adsorbent is relied upon the surface chemistry, and hence much of the research attention in the recent past is devoted towards the chemical modification of the sorbent surface.

Through this chemical modification induce additional functional groups such as amine, amides, carboxylate, hydroxyl, phosphate ions. These additional functional groups induction will enhance the surface properties such as porosity, surface roughness and better adhesion possibility with effective adsorption capacity. Further, the most common chemical treatments include, CTAB modification, acid treatment, grafted co-polymerization, calcination etc. But very few attempts were made to functionalize the natural adsorbents via green solvents room temperature ionic liquids (RTIL). As an alternating medium of extraction, ILs have taken on significant importance due to its intriguing properties, such as low vapor pressure, non-volatility, flammability, broad electrochemical properties and high conductivity of ions. [9]. Moreover, Imidazolium ILs are most prevalent as surface modifiers as they promote the electrostatic, ion exchange, π-π interactions between the sorbate and sorbent. The combination of chelating agents and extraction, all of which together are reflected as a partition of different stages, is one of recent efforts to separate metals ions from different matrices via RTIL [10]. Crown ethers N-alkyl aza-18-crown-6 series, calix [4] arene-bis(*tert*-octylbenzocrown-6) combined with RTILs to extract Cs^+ and Sr^{2+} from aqueous solutions [11], RTIL combined bmimPF6-dithizone metal chelator for the extraction of heavy metals from aqueous solution into bmimPF6 [12] were some examples. In continuation, calix [4] arene-bearing pyridine with 1-alkyl-3-methylimidazolium PF6 for the Ag + extraction [13], 8-sulfonamidoquinoline chelating derivatives with 1-butyl-3-methylimidazolium hexafluorophosphate [14] [bmim][PF6] for divalent metals, fluorous ionic liquids with macrocyclic polyethers [15] were some of the recent explorations. Another study revealed 1-butyl-3-methylimidazolium bis (trifluoromethylsulfonyl) imide combined with N,N-dioctyldiglycolamic acid (DODGAA) forming a resin to separate lanthanides [16], and as a surrogate in CO_2 separation [17] etc. However, the major disadvantage using RTIL is finding suitable chelating compound specific to the metal ions. These chelating agents binds the metal ions and transfer their matrices to the IL medium during the complexation stage.

Hence, the present study aims to formulate a new adsorbent medium Hazel *Sterculia Foetida L.,* (HS) mediated with 1-butyl-3-methylimidazolium bis (trifluoromethylsulfonyl) imide avoiding any chelating agents. Furthermore, the newly synthesized HS-IL adsorbent was tested its applicability in separating Pb and Cr ions from the aqueous streams and the results were compared to the raw HS adsorbent. Through this comparison study, one can clearly elucidate the impact of the IL as a surface modification agent enhancing the adsorption capability. Finally, till date many IL based adsorbents were synthesized, but no attempt was made combining natural seed material (HS) combined with IL which makes this a new adsorbent variant added to the database.

2. Experimental

2.1. Materials and methods

The raw material HS was obtained from the surroundings of the National Yunlin University of Science and Technology. Ionic liquid, reagents, and chemicals used in this study were of analytical grade supplied by Sigma-Aldrich Taiwan require no further purification process:

1-butyl-3-methylimidazolium bis(trifluoromethylsulfonyl) imide, methanol, NaOH (≥99%), HCl (≥37%), $NaAlO_2$, KOH, HNO_3 (>99%), CH_3OH (99.8%), C_2H_5OH (≥99.5%), $Pb(NO_3)_2$ (>99%), $K_2Cr_2O_7$ (99.9%), Diphenylcarbazide, H_3PO_4 (>99%), 1–5, diphenylthiocarbazone (>98%), CCl_4 (>99.5%).

2.2. Preparation of adsorbent

Two adsorbent materials, raw HS, IL functionalized HS, were considered in the present study to test the adsorption ability of Pb (II), Cr (VI) from the aqueous solution. To start with, HS and IL were combined in the ratio of 1:2, and the slurry was agitated in a magnetic stirrer maintained at 500 rpm for six hours. The resultant slurry was highly viscous, and a known property of IL tends to retain the liquid phase at ambient room temperature. Further, to obtain the amorphous IL functionalized, HS seed powder was dispersed in organic solvent (methanol) and stirred at 500 rpm for three h. Finally, the solid form of IL functionalized HS seed powder was obtained, heated at 40 °C for two days to stabilize the structure. Then, the synthesized solid form was finely ground to powder and stored at control temperature conditions to avoid functionality losses.

2.3. Characterization techniques

2.3.1. Xrd

Bruker Advanced D825A X-ray diffractometer has been used to record the crystallographic aspect of adsorbents, i.e., raw HS, IL-functionalized HS. Patterns of 0.02 counts per second were recorded in the 2θ range of 5°–60° with Cu-Kα radiation at 40 kV and 40 mA.

2.3.1.1. BET measurements. HS-IL adsorbents were examined in a surface-pore-size analyzer for the textural properties by nitrogen (N2) adsorption technique (Micrometrics, ASAP 2060). The samples were degassed at 150 °C overnight (12 h) as standard operating procedure before the analysis. Further, the specific surface areas of the adsorbents were evaluated by the standard Brunauer-Emmet-Teller (BET) method and the pore-related information via Barrette-Joyner-Halenda (BJH) method.

2.3.1.2. SEM picture modeling. To assess the surface morphology, the adsorbent samples were coated with gold with the help of a sputter coater for 150 sec to enhance the conductivity. Later, the samples were evaluated for the morphological aspects via Ultra-High-Resolution Thermal Field Emission Scanning Electron Microscope (JEOL, JSM-7610F Plus) under vacuum at 25 kV tungsten filament.

2.3.1.3. FTIR analysis. FTIR spectra were recorded with Fourier transform infrared spectroscope (FTIR, PerkinElmer spectrum One) to reveal the functional group's presence in the adsorbents. The functional group detection with the DTGBr detector was done in 400–4000 cm^{-1} and KBr split beamer had been scattered in a 200 mg KBr spectroscopic class to record the spectrum before the dried sample weighing 10 mg.

2.4. Batch adsorption experiments

The batch adsorption studies determined the adsorption behavior of Cr (VI), Pb (II) onto HS, HS-IL. The present batch adsorption studies were performed in 100 mL Erlenmeyer's flasks, with fixed initial metal solution concentrations Cr (VI), Pb (II) of 300 ppm,

and the volume of 30 mL, respectively. Initially, the pH of the metal solutions was optimized by taking 30 mL of each metal solution separately and adjusting to optimal pH via adding appropriate quantities of 0.1 N HCl acidic solution and 0.1 N NaOH alkali solution in the range of 2–10. Once the pH of the solution was optimized, the point of zero charge tests was performed using the appropriate addition of 0.1 N HCl acidic solution and 0.1 N NaOH alkali solution in the range of 2–10.

2.5. Cr (VI) color development method for UV–vis spectrophotometer

The standard method (CR-3500) was used to determine Cr (VI) in the prepared solution using a UV–vis spectrophotometer, and the procedure was detailed in our previous studies [2]. Initially, Diphenylcarbazide dye solution was prepared and tested the absorbance via UV–vis at a wavelength of 540 nm as a typical procedure. Further, a calibration curve at λ_{max} = 540 nm was prepared using serial dilutions from 0.5 to 5 μg/L of different volumes (1, 2, 5, 7, and 10 mL), respectively. Next, the pH of the solutions was adjusted to 2.0, and then the solution was transferred to a 100 mL volumetric flask. Upon transfer, the solution was added with already prepared phosphoric acid (H_3PO_4) dropwise and 2 mL of prepared 1,5-diphenylcarbazide solution. The solution was further stirred thoroughly for 5 to 10 min till the red-violet color developed. Finally, transfer the color solution to the quartz cell with a path length of 1.0 nm and evaluate the absorbance by UV–vis spectrophotometer (Perkin-Elmer Lambda 850) at the wavelength of 540 nm.

2.6. Pb (II) color development method for UV–vis spectrophotometer

The change of Pb (II) ion concentration due to adsorption was determined by UV–vis spectrometer. Dissolve 159.9 mg of Pb $(NO_3)_2$ in de-ionized water to 100 mL of stock solution (1 mg/mL) for divalent lead. One of the most commonly used photometric reagents and forms colored water-insoluble complexes with many metal ions is the 1–5 Diphenylthiocarbazone (dithozone).

Metal-dithizone complexes are water-insoluble, and thus a prior solvent extraction step into chloroform or carbon tetrachloride is necessary for their determination. By dissolving the required amount (0.005 percent) of diphenythiocarbazone in a known volume of 2-propanol, the standard dithizone solution was prepared. The 1–5, diphenylthiocarbazone in ammonia in alkaline form has developed a brick-red-color solution complex. At a wavelength of 530 nm, absorption was measured. The amount of the Cr (VI), Pb (II) metal ions adsorbed onto the surface of the HS, HS-IL were calculated according to the mass balance of the metal ions concentration eq. (1), and the percentage of the desorption was calculated by eq. (2) respectively.

$$q_e = \frac{(C_i - C_e)V}{m} \quad (1)$$

$$\text{Desorption}(\%) = \frac{desorption}{adsortpion} \times 100 \quad (2)$$

3. Results and discussion

3.1. XRD and SEM analysis

The diffractogram outlines the crystallinity and structures of samples by way of the XRD method. Additionally, XRD analysis reveals the orientation of crystals in the samples. The XRD patterns of the raw HS and HS functionalized ILs are shown in Fig. 1. The raw HS's XRD patterns before functionalization indicate the inference peaks at 2θ = 26.39°, and 34.50° respectively. As the selected raw adsorbent (HS) is an organic sample obtained from plant waste, the major constituents are cellulose, which was confirmed through the peak of 34.50° [18] regarding the characteristics of the plane (040). Further 26.39° [19] denotes the existence of the carbon content with a plane (002) in HS seed powder. Upon functionalization with ionic liquid, there was the peak observed at 2θ = 26.34° [20], representing intense crystallization demonstrating the ion association and coagulation to lead the decrease in conductivity. Another low intense peak at 34.41° denoting the carbon phase. This summarizes that the intensity was the main difference observed with functionalization, which means before IL addition, the nature of the material was amorphous. In contrast, the IL intensified the structure to become a crystalline structure.

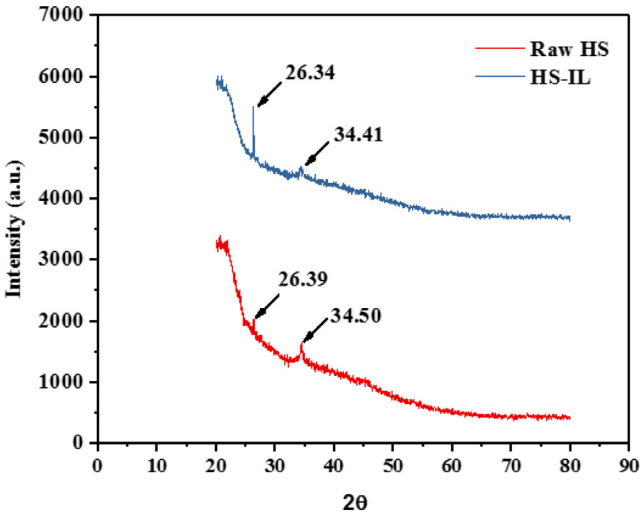

Fig. 1. XRD spectra of raw HS, HS-IL.

Further, the surface morphology of raw HS and IL functionalized HS were evaluated with a scanning electron microscope, and the respective images are presented in Fig. 2. From Fig. 2 (a, b), it is seen that the particles of HS are randomly distributed, irregular and heterogeneous with no specific shape reported. However, the functionalization tends the particles to be intertwined, forming a cross-linked framework probing dense agglomerates Fig. 2 (c, d) on HS binder with IL. Furthermore, after adding ionic liquid, the surface cavities tend to be streamlined by the occupancy of the ionic liquid on the irregular surfaces of Hazel *Sterculia Foetida* L. surface, thereby forming porous, smoother homogeneous cavities. These structural properties of the adsorbent expedite its interaction with an adsorbate.

3.2. BET analysis

As can be shown in Fig. 3 (a, b), HS and HS-IL showed good N_2 adsorption capability. On the other hand, the IL-functionalized HS used in the N_2 adsorption capacity experiment had a greater surface quality than untreated HS. This is due to the increased specific surface area of HS-IL compared to HS, and the details are presented in Table. Further, the figure confirms the Type II isotherm suits both HS and HS-IL adsorbents more appropriately. When adsorption occurs on nonporous materials with pore dimensions bigger than micropores, Type II isotherms are more prevalent. For this case, the knee point of the isotherm, where the relative pressure changes and where the first adsorbed monolayer is completed, is usually located around the start of the first adsorbed layer. From there, more adsorbed layers are formed until the point of saturation, where the number of adsorbed layers is infinite. [21]. More-

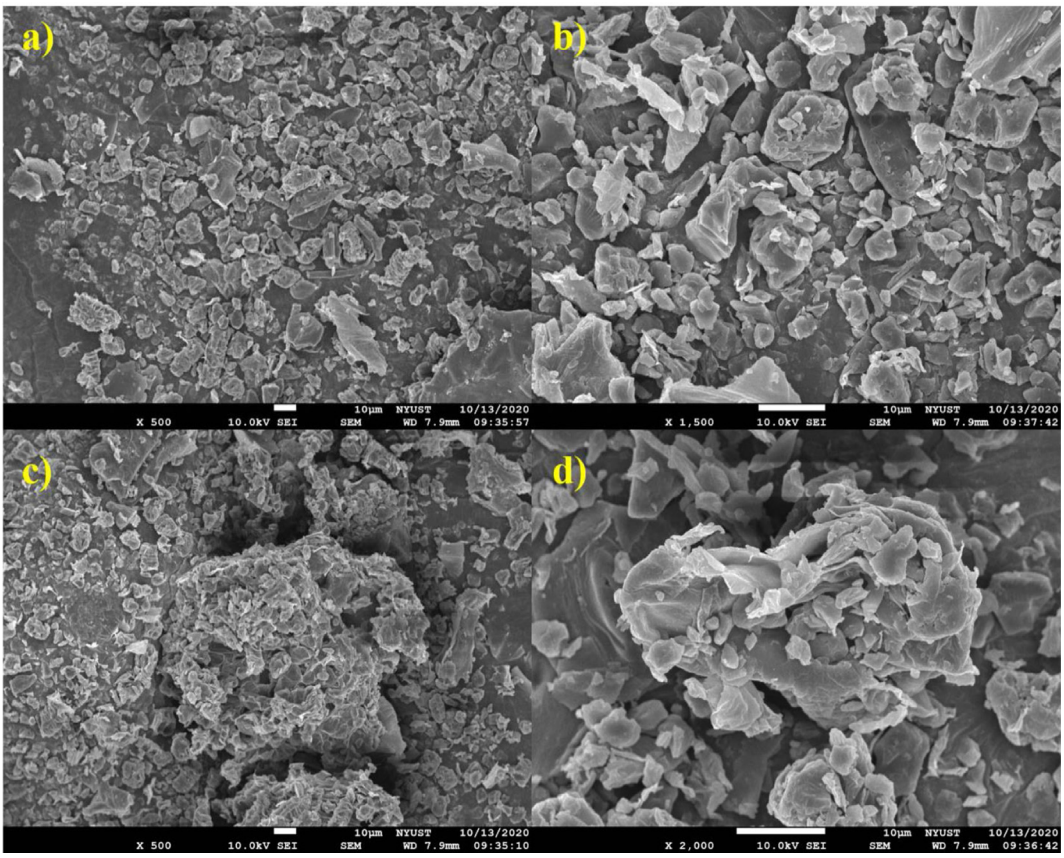

Fig. 2. SEM micrographs of (a, b) raw HS; (c, d) IL functionalized HS (HS-IL).

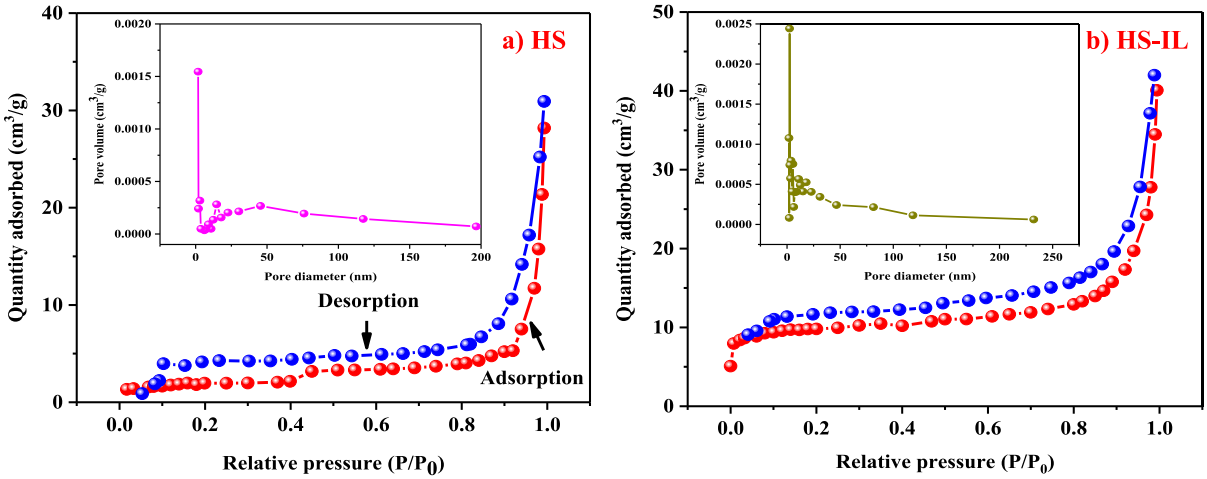

Material	BET area (m^2/g)	Surface area SA_{ext} (m^2/g)	V_{micro} (cm^3/g)
HS	9.711	3.462	0.060
HS-IL	30.14	8.984	0.19

Fig. 3. N_2 adsorption–desorption isotherms, BJH pore size distribution (onset) of a) raw HS; b) HS-IL and the corresponding surface areas of both the adsorbents.

over, the Hysteresis defines the divergence between the adsorption and desorption nature of the system which may not coincide. Hence, Fig. 3 (a, b-inset) represents such discrepancies of adsorption and desorption, indicating the H3 hysteresis loop. This H3 hysteresis confirms micropores of non-uniform size and is more commonly found on solids with a very wide distribution of pore sizes. Furthermore, the BET report suggests that the functionalization of HS with IL substantially improved the pore characteristics by three folds from 9.711 m^2/g to 30.04 m^2/g. Further, the pore volume of the raw HS is reported to be 0.060 cm^3/g has been increased to 0.19 cm^3/g respectively. This enhanced pore volume and the surface area is due to the unobstructed movement of N_2 passage

through the pores enhancing both the surface area and volume for better entrapment.

3.3. FTIR analysis

Fig. 4 shows the FTIR spectrum of the raw HS, the ionic liquid functionalized HS (HS-IL), and their respective functional groups. The information facilitates the analysis of the responsible functional groups tending the sorbate molecule's adsorption onto the sorbent surface. It is observed from Fig. 4a that the raw HS, i.e., before RTIL functionalization, possess intense peaks in the range of 1000–3000 cm^{-1}. The peaks at 1010 cm^{-1}, 1206 cm^{-1} [22], signifies the stretching and bending vibrations of (C–O), 1360 cm^{-1} represents bending vibrations of (C–H) [23], 1710 cm^{-1} identified as vibrational mode of carboxyl groups [24], 2854 cm^{-1} indicates (CH_2) vibrations, and 2924 cm^{-1} denotes the stretching vibration of alkyl groups (C–H) [25] respectively. After RTIL functionalization, significant changes in functional groups of the newly prepared adsorbent (HS-IL) with broad range of new peaks (Fig. 4b). The figure shows the intense formation of new peaks in the range of 400–1000 cm^{-1} and 1000–2000 cm^{-1}. The major identifications were 485 cm^{-1} indicating the presence of OH groups, 570 cm^{-1}, 650 cm^{-1} is the confirmation of pure TFSI IL, 612 bending vibrations of sulfonyl (SO_4^{2-}) groups existing in IL [26], 740 cm^{-1} attributes alkyl chains [27], 790 cm^{-1} as C = O bonds. Further, the peaks at 1053 cm^{-1}, 1132 cm^{-1} [26], 1182 cm^{-1}, 1348 cm^{-1} (S = O) [28], 1711 cm^{-1} were designated as twisting NCH_3 [29], asymmetric stretching of SO_4^{2}, in-plane deformation vibration of imidazolium ring [30], and the vibrations of ester groups involved in hydrogen bonding respectively. Finally in the range of 2000–4000 cm^{-1} there were two peaks identified at 2928 cm^{-1} [31], 3160 cm^{-1} ascribing the asymmetric stretching of C-H bonds and symmetric stretching of HCCH present in the imidazolium ring [32], and the presence of amino groups (NH_2) from HS seed [33], respectively. Thus, from this FTIR analysis, it is clear and confirmed that IL is well bound or functionalized onto the surface of the HS, thereby altering the functional groups followed by the physico-chemical characteristics of the adsorbent material.

3.4. Effect of pH

The pH is the key aspect that plays a vital part in speciation on the adsorbent surface of functional groups which define the solubility of sorbate molecules inside an aquatic surface. Further, the adsorption potential is altered, i.e., enhance or deduced by varying the ionization state, and hence regarded as the master variable in any adsorption phenomenon. For instance, Pb in an aqueous medium can exist as either $Pb(OH)^{+}$, Pb^{2+}, $Pb(OH)_2$, $Pb(OH)^{-3}$; Cr as $Cr_2O_4^{2+}$, $HCrO_4^{-}$, $Cr_2O_7^{2-}$ etc.; all of which are solely relied on the pH of the solution. In order to analyze the effect of pH, tests with beginning pH values between acidic and alkaline (0 < pH < 10) were therefore carried out under optimum parameters (dosage, temperature, agitation speed, contact time). The solution pH is well supported by adding 0.1 N HCl in the acidic medium and 0.1 N NaOH for alkaline solutions. Fig. 5 demonstrates the influence of solution pH on the adsorption of Cr (VI), Pb (II) onto HS, HS-IL respectively. From Fig. 5a it is observed that the adsorption propensity of Cr (VI) towards HS, HS-IL increased until pH = 3 and declined further, increasing pH. Similar behavior was seen by the Pb (II), i.e., the metal uptake onto HS, HS-IL increased until pH = 5 (Fig. 5b). In the alkaline medium, adsorption declined very steeply or attained equilibrium. The maximum metal uptake by the adsorbent at the optimal pH values reported were 28.7 mg/g, 62.8 mg/g (Cr (VI)), and 33.9 mg/g, 84.7 mg/g for Pb (II) towards HS, HS-IL. The decreasing sorption with increasing pH is due to; at pH > 6, hexavalent Cr exists in CrO_4^{2-} containing larger number of hydronium ions hindering the diffusion of chromate ions, so the removal decreases [34]. Similarly, the decreasing nature of adsorption with increasing pH is due to the formation of soluble hydroxyl complex of $Pb(OH)_2$ [9]. Another reason for lower

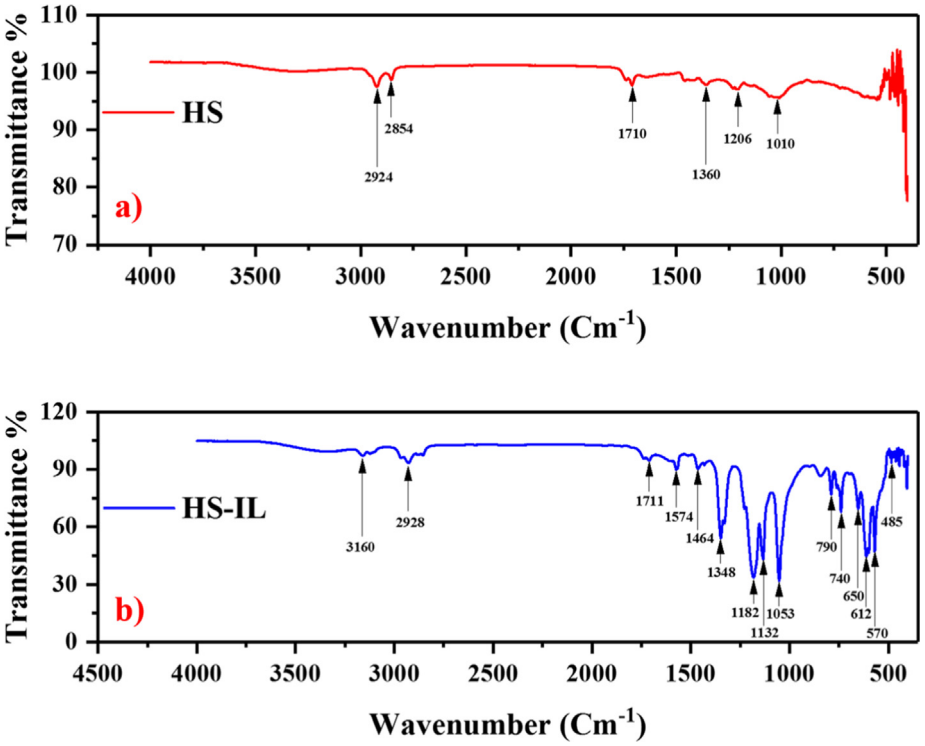

Fig. 4. FT-IR spectrum of raw HS, and modified HS with ionic liquid.

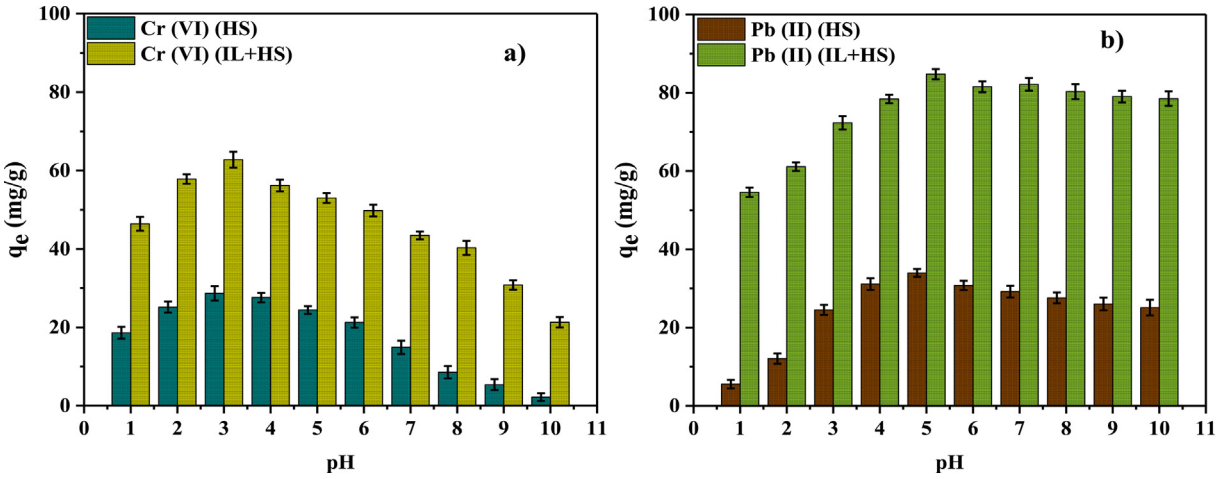

Fig. 5. Effect of pH on the adsorption capacity of using HS, HS-IL; a) Cr (VI), b) Pb (II).

adsorption in IL-modified sorbents at low pH might be the protonation of functional groups (NH_2, COOH) containing lone pairs. As the pH increases, the lone pairs of oxygen and nitrogen atoms in functional groups of adsorbate develop stronger electrostatic interactions, which result in metal ions adsorption [35]. Thus, the optimum sorption of ionic liquid-functionalized sorbents of metal ions Cr (VI), Pb (II) is pH = 3, 5 and the same pH has been retained throughout the investigation.

Further, the effect of pH, surface charge variations affecting adsorption process can be assessed by point of zero charge analysis (pH_{pzc}), the point at which the net charge of sorbent molecule remains zero. The point of zero charge process was clearly established [36] begins by considering 0.01 M NaCl solution, adjusting pH via 0.1 HCl and 0.1 N NaOH mediums, respectively. The solution medium was then agitated at 200 rpm (Cr (VI)), 300 rpm (Pb (II)) for a period of 2 h (Cr (VI)), and 3 h (Pb (II)) at 303 K, respectively. Once the solutions' pH was stabilized, the final pH (pH_f) was noted, and the gradient of pH_i, pH_f was plotted against pH_i (Fig. 6). The adsorbent surface was neutral (pHpzc) at the pH inflection point of value 7.11 (HS) and 7.89 (HS-IL), which is the pH < pHpzc for the adsorption with Cr (VI) and Pb (II). At solution pH lower than pH_{pzc}, methylimidazolium ionic liquid rings and protonated secondary amine groups bore positive charges. These positive and negative charges result in anionic hexavalent Cr or divalent Pb, which is more or less prepared for adsorption, to electrostatically attract or repel.

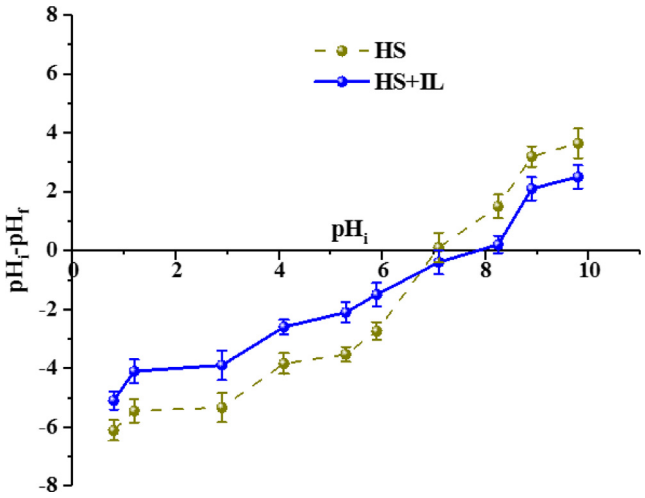

Fig. 6. Effect of pHpzc on the adsorption capacity of using HS, HS-IL.

3.5. Adsorption mechanism

Fig. 7a represents the interaction of the biomass waste (HS) with main component cellulose interacting with the ionic liquid 1-butyl-3-methylimidazolium bis (trifluoromethylsulfonyl) imide. From the FTIR studies, it is evident that HS-IL undergo three major interactions namely; amination, esterification, sulfation resulting esters, sulfates, and amine, while carbon groups tend to disappear after interaction. The observed adsorption mechanism from Fig. 7 b can be attributed to the electrostatic interaction of positive charged elements with negative metal ions in the lower pH solution. For the properties and dynamics of the adsorption phenomena, hydrogen bonding plays a vital role. FT-IR and pH studies can assign the detailed adsorption phenomenon. The results of pH illustrate the effect on extraction recovery of Cr (VI), Pb (II) as it not influences the surface-active centers alone. pH also impacts the degree of ionization, ionic strength, and solubilization of the sorbate in aqueous solutions. This means that increasing the ionic strength increases, the electrostatic interaction between the ILs and the analytes in solution reduces the extraction recovery. Furthermore, IL-functional HS adsorbent particles might be linked to Pb (II) extraction, namely: the direct contact of metal ions with ILs, the interaction between the surface functional groups and the metal ions could be an ion exchange connection. The functional ILs comprising the oxygen and nitrogen pairs produce strong electrostatic interactions with sorbate ions that lead to considerable adsorption of metal ions, Pb (II). In case of Cr (VI), protonation decreases or deprotonation with the increasing pH resulting liable to the continuous downfall of electrostatic interactions between the adsorbate and adsorbent, also the concentration of OH^- increases, thereby competitive adsorption of CrO_2^{4-}. At pH values around 2, the dominating form of chromium is $HCrO^{4-}$, which is populated by a significant number of H^+ ions. When pH increases, $Cr_2O_7^{2-}$, CrO_4^{2-}, $HCrO_4^-$, compete for adsorption sites [37]. In addition, the solution's concentration of OH^- ions results in chromate and hydrogen chromate ions having to compete for adsorption, and an electrostatic repulsion event can occur as a result. The chemisorption aspect of adsorption arises from electrostatic interactions [38].

Furthermore, the takedowns from FT-IR studies denotes the interaction between the sorbate and sorbent molecules are due to the presence of C-H and –OH bonds. The presence of these bonds

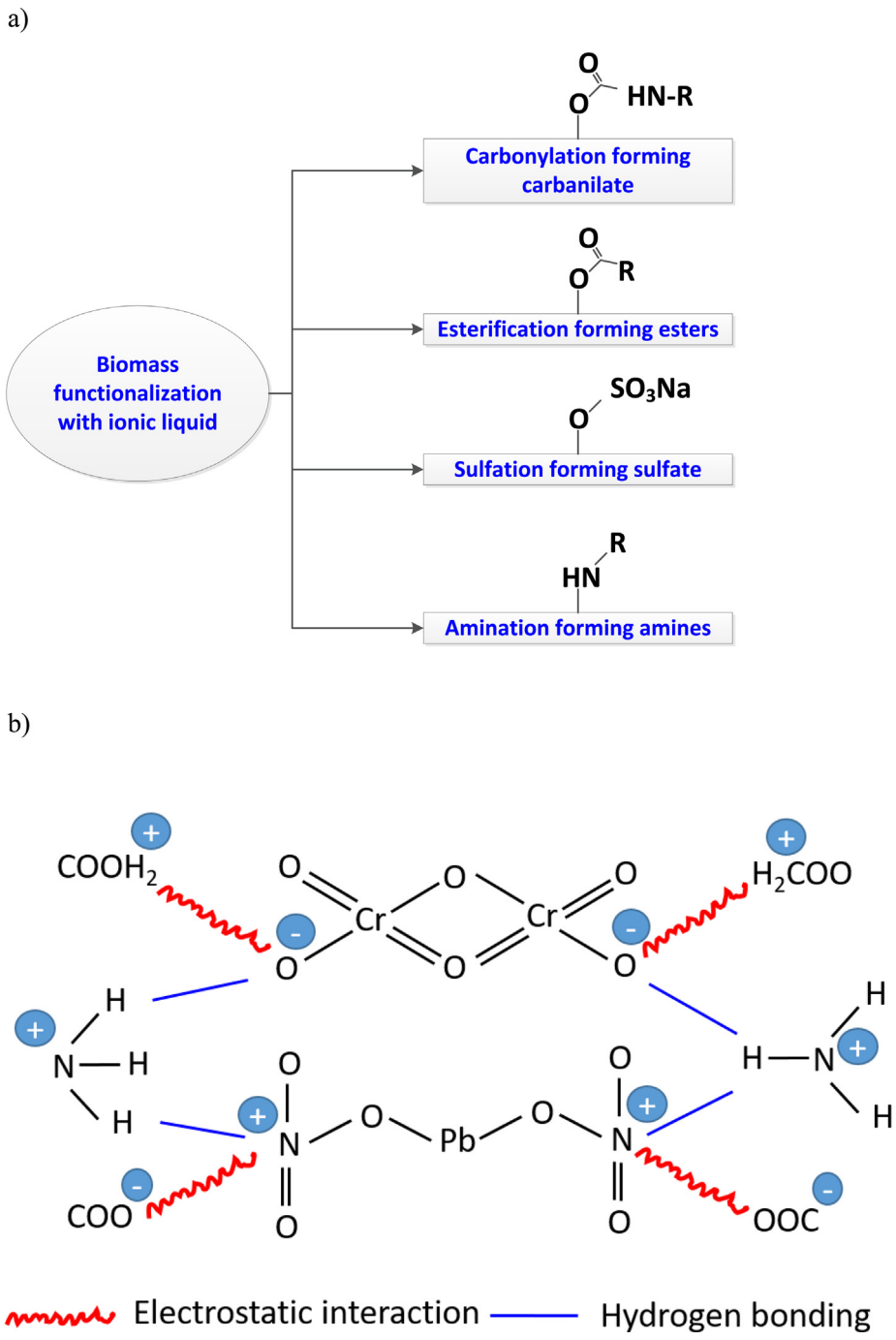

Fig. 7. a) interaction of the biomass (HS) with IL (1-Butyl-3 methylimidazolium bis(trifluoromethylsulfonyl)imide); b) Adsorption mechanism of Cr (VI), Pb (II) onto HS-IL.

will result in the hydrogen bonding between the sorbate and sorbent molecules, thereby enhance the adsorption phenomenon. Moreover, the prevalence of the hydrogen bonding trend in imidazolium-based ILs is indicated by short anionic C-H distances, red shifted C-H stretching frequencies and downfield shifted C-H proton chemical shifts. In addition, the C-H vibrational stretching vibrations, electronegative N of IL forming H_2 with OH^- [39] on HS elucidates the prevalence and strength [32] of the hydrogen bonding, and also the trend towards immobilization. There may be two more reasons for adsorption of Cr(VI) metal ions, namely the occurrence of a 3d empty orbital and the formation of a coordinating link with the compound of an IL oxygen atom lone pair of electrons to the metal center [40]. Secondly, in the HS-IL structure, –OH groups can make strong hydrogen connections to Cr (VI) ions compared to those produced by the hydrogen interlinkages between water and metal ions [41]. For Pb (II), the Pb^{2+}, [Xe] $4f^2 5d^{10} 6s^2$ electron configuration includes a 6 s^2 electron pair that can either be stereo chemically active or inert molecule. The valence shell electron pair repulsion theory (VSEPR) explains that less significant bonding activity is exhibited by S-orbitals for heavier molecular species, and hence more electron density will be present in the space between the atomic nuclei. A mostly spherical orbital will be the primary home of a set of static electrons i.e., a pair of lone electrons. Because the p-orbitals are directed in nature, the location of a lone pair is not important, and the Pb-O bond formation is thus boosted [42]. Hence, the metal cation will bind the

polymer-metal complex and precipitate it from the solution and can be filtered, separated. The inorganic anions in the IL were replaced by Cr (VI) and Pb (II) after the adsorption of Cr (VI) and Pb (II), respectively. The Cr (VI) and Pb (II) present in the aqueous stream, however, adsorbed to achieve the removal of heavy metal ions from water [39].

Summarizing, the overall chemistry, mechanism of the adsorption separating the Cr (VI), Pb (II) using HS-IL involves a complex phenomenon, however, the selected adsorbent is more selective in separating Pb (II) than the Cr (VI).

3.6. Influence of adsorbent dosage

The number of active sites on the adsorbate is controlled by the amount of the adsorbent dosage, and hence a crucial aspect to deal with especially in adsorption studies. Another significant importance of the dosage studies is to avoid the excess consumption of adsorbent, a key factor of process economics. Hence, the effect of the adsorbent dosage on the adsorption efficiency for Cr (VI), Pb (II) on HS, and HS-IL was studied at room temperature of 303 K with different sorbent doses (0.05–0.4 g) in 30 mg/L aqueous solutions maintained at optimal pH values (Fig. 8). In case of the Pb (II), Cr (VI) treated with HS, the sorption tendency was reported as 31.2 mg/g at 0.4 g, and 26.5 mg/g at 0.1 g respectively. However, IL functionalized HS reported similar tendency of increasing sorption with increasing dosage and found optimal as 87.3 mg/g at 0.4 g for Pb (II), and 63.8 mg/g at 0.1 g for Cr (VI) respectively. As the adsorbent dosage increased, the adsorption became more prevalent, mostly due to an increase in accessible active sites on the surface of the adsorbent [43]. Once, attaining the equilibrium there the sorption process commensurate with the adsorbent dosage which is likely due to superficial adsorption onto adsorbent producing a lower solute concentration in the solution [44]. In addition, the equilibrium is due to the presence of large number of accessible surface active groups than the adsorbate amount [45]. In summary, the optimal dosage was fixed as 0.1 g for Cr (VI) using HS, HS-IL, and it was 0.4 g for Pb (II) dealing with HS, HS-IL throughout the study.

3.7. Influence of agitation speed

The adsorption phenomenon's speed of agitation is another important variable, which has a stronger effect on the solute's distribution in the bulk solution. This investigation on the effects of agitation rate on Cr (VI) and Pb (II) Cr (VI) and Pb (II) found that at 303 K and pH = 3 and pH = 5, respectively, the latter runs at 100–500 rpm and the former runs at 300 rpm for Cr (VI) and HS, HS-IL (0.1 g) and HS, HS-IL (0.4 g) for Pb (II) for 60 and 120 min, respectively. From Fig. 9 there observed an increasing adsorption tendency of Cr (VI), Pb (II) onto HS, HS-IL at lower speeds (100–300 rpm), and declining or attaining equilibrium at higher agitation speeds (300–500 rpm). Further, the Cr (VI) uptake on HS, HS-IL at optimal agitation speed of 200 rpm was reported to be 26.6 mg/g and 61.4 mg/g (Fig. 9a). Whereas, the sorption of Pb (II) onto HS, HS-IL at optimal agitation speed of 300 rpm was reported as 33.7 mg/g, and 83.7 mg/g respectively (Fig. 9b). The increasing adsorption at lowers agitation speeds probes sufficient contact between adsorbate Cr (VI), Pb (II) and adsorbent (HS, HS-IL). Additionally, the boundary layer around the particles facilitates the diffusion of the adsorbate to the adsorbent, which boosts the external film transfer coefficient and hence the removal of adsorbate, resulting in a higher percentage of adsorbate extraction [46]. Beyond the optimal agitation speed the increased turbulence lowers the boundary layer thickness, adsorbate species experiencing greater centrifugal forces detaches from the sorbent surface resulting the drop of adsorption capacity [47]. The equilibrium sorption of adsorbate onto adsorbent is a resultant of insignificant effect of the agitation speed on the film thickness. Thus, 200 and 300 rpm were chosen as optimal speeds for sorption of Cr (VI), Pb (II) onto HS, HS-IL and maintained the same throughout the present study.

3.8. Effect of contact time on metal ions adsorption

In order to design the mode of adsorption phenomenon, one key variable has to be accounted for is the contact time of adsorbate and adsorbent. A series of batch trails were completed to assess the effect of contact time (0 to 300 min), metal concentration (50 mg/L Cr (VI) and Pb (II)), dosage (0.1 g Cr (VI) and 0.4 g Pb (II)), and pH (3 for Cr (VI) and 5 for Pb (II)) and temperature (303 K) on HS, HS-IL, and agitation speed (200 rpm for Cr (VI) and 300 rpm for Pb (II)). The effect of contact time on adsorptive removal of Cr (VI) and Pb (II) from HS, HS-IL is shown in Fig. 10 (a, b). The results showed that Cr (VI) crossed the phase barrier in less than a half hour; and the same amount of time was needed for Pb (II) during the initial stages (0–30 min); and (0–45 min) for Pb (II). This rushing adsorption was due to the diffusion of sorbate molecules diffusing onto the active vacant pore sites of sorbent

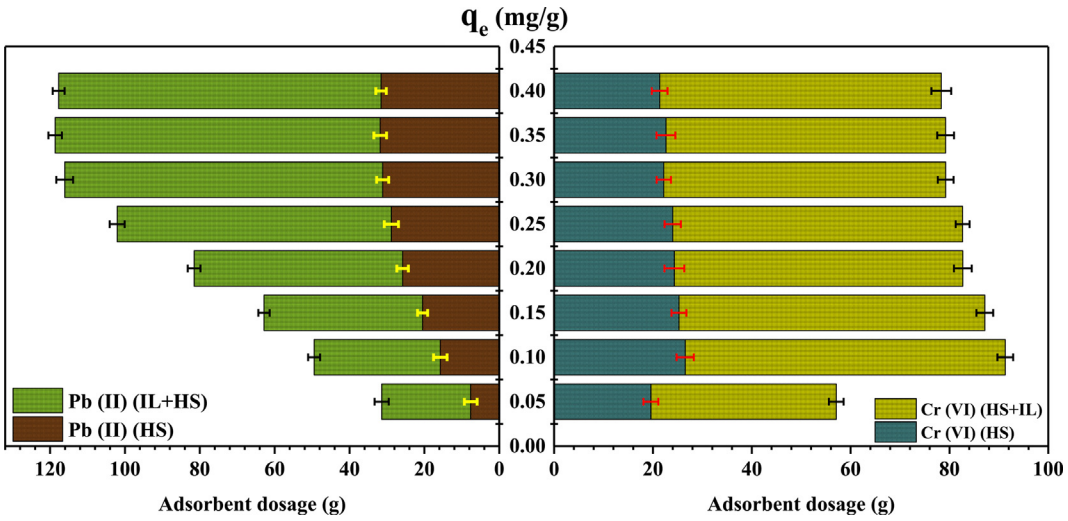

Fig. 8. Effect of adsorbent dosage on the adsorption capacity of Cr (VI), Pb (II) onto HS, HS-IL.

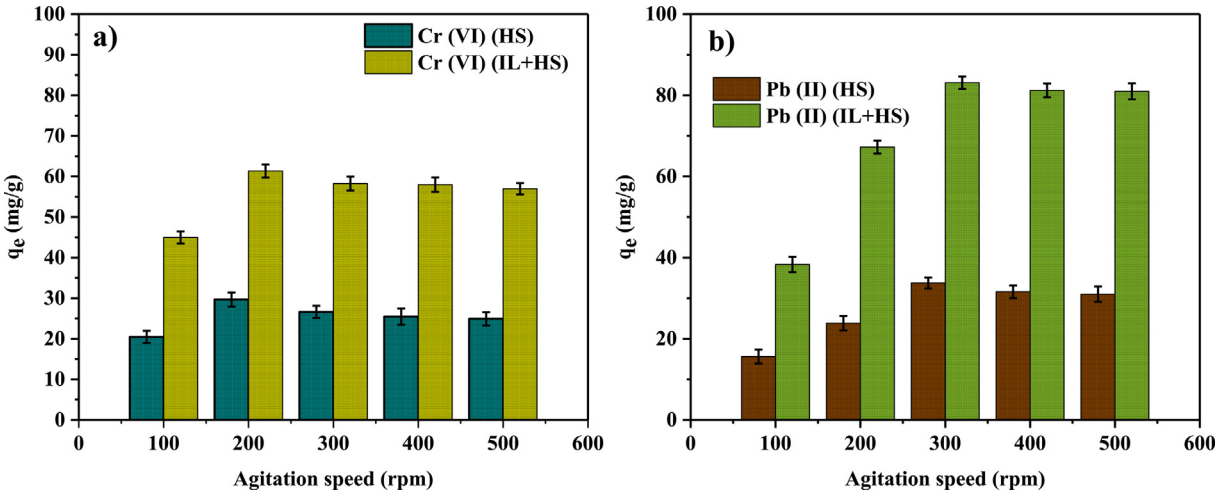

Fig. 9. Effect of agitation speed on the adsorption capacity of using HS, HS-IL; a) Cr (VI), b) Pb (II).

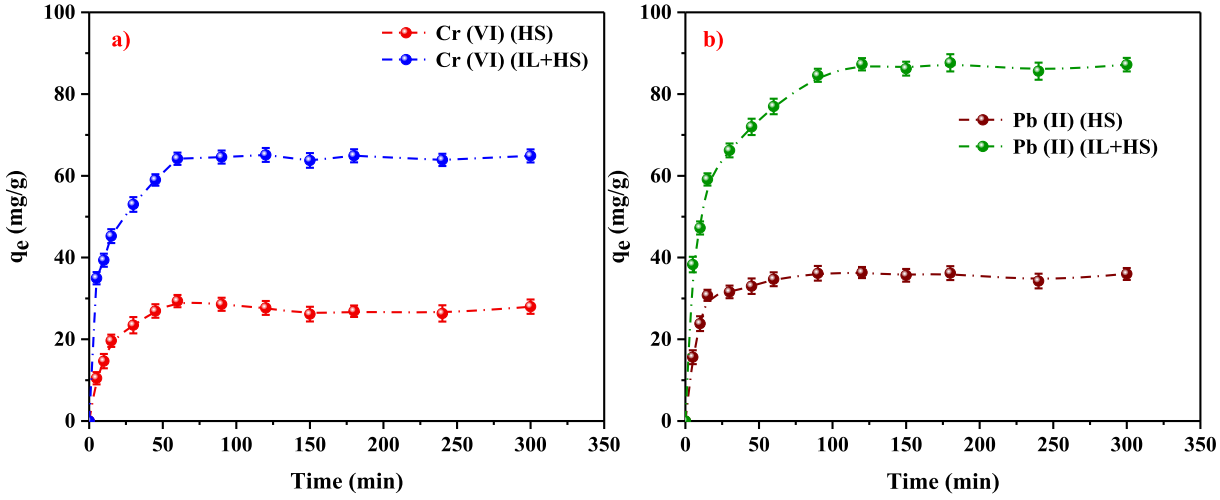

Fig. 10. Effect of reaction time on the adsorption capacity of using HS, HS-IL; a) Cr (VI), b) Pb (II).

molecule. Increasing the contact time the sorption of Cr (VI) was gradual in the timeline of (30–60 min); and for Pb (II) it was (45–120 min). This linear increment is an indication of multilayered lumping, and saturation of vacant sites. Further, increasing the time beyond 90 min for Cr (VI), and 120 min for Pb (II), there observed a flat plateau with maximum adsorption of 28.4 mg/g, 64.2 mg/g for Cr (VI); and it was 37.3 mg/g, 87.3 mg/g for Pb (II) onto the sorbents HS, Hs-IL respectively. The plateau is the resultant of flushing out the sorbate molecules due to the completely filled sorbent pores. Hence, the optimal contact time was considered as 60 min, 90 min for the adsorption Cr (VI), and Pb (II) in the entire study.

3.9. Adsorption isotherms

To make the best use of adsorption systems, the study of adsorption isotherms is a need. The information they offer is useful for understanding the dynamic separation of solute from solution that occurs on the adsorbent under equilibrium conditions. Adsorption isotherms govern the balance between adsorbate, adsorbent, and the bulk liquid. To explain the HS, HS-IL, adsorption capacity, the experimental equilibrium data were evaluated according to the Langmuir, Freundlich, SIPS, and Toth models at 303 K.

4. Langmuir isotherm model

The Langmuir isotherm model is accurate in describing the monolayer sorption of solute from solution to the identical sites on the surface of the adsorbent. Further, the model is functional on the following assumptions; the sorption process is carried out at specific homogeneous sites upon which the sorbate molecule is rested on. All the vacant sites are identical and possessing equivalent energy; upon filling the sites presumed that the finite capacity of the adsorbent has reached equilibrium [48]. The mathematical expression of the Langmuir isotherm model in its non-linear form is expressed as:

$$\text{Langmuirisothermmodel}: q_e = \frac{q_m K_L C_e}{1 + K_L C_e} \quad (3)$$

The equilibrium, and maximum adsorbate liquid-phase concentrations (mg/L) of the HS and HS-IL adsorbent and the amount of Cr (VI) and Pb(II) adsorbed on HS were denoted by the variables q_e, q_m, C_e, respectively. K_L is Langmuir equilibrium constant (L/mg)

represents the possibility of adsorption process i.e., $K_L > 1$ unfavorable, $0 < K_L < 1$ favorable. The Langmuir isotherm plot of Cr (VI), Pb (II) adsorption onto HS, and HS-IL were shown in Fig. 11 (a-d). Table 1 presents all the key variables that were modeled through various isotherms the higher degree of linearity was seen as the regression coefficient of 0.9974, 0.9985 for HS, HS-IL respectively. Moreover, the experimental values (q_e) were in close proximity with the model values (q_m) and reported as 29.2 (mg/g), 36.4 (mg/g) for Cr (VI), PB (II) adsorption on HS, and 82.9 (mg/g), 108.6 (mg/g) for Pb (II) onto HS-IL respectively.

4.1. Freundlich isotherm model

The Freundlich isotherm, as previously stated, accounts for heterogeneous sorption systems with disparate energy levels for the multilayer sorption sites [49]. The non-linear form of the Freundlich isotherm equation has the following mathematical expression:

$$\text{Freundlichisothermmodel}: q_e = K_f C_e^{1/n} \quad (4)$$

The variables q_e (mg/g), C_e (mg/L), K_f (L/mg), 'n' from the equation were the equilibrium adsorption capacity, equilibrium concentration, Freundlich energy constant, and adsorption intensity respectively. Among these variable "n" defines the favorability of the reaction based on the following condition ($1 < n < 10$). The Fig. 11 (a-d) shows how the theoretical Freundlich isotherm model data compares to the experimental equilibrium data. The numerical predictions of the adsorption of Cr (VI), Pb (II) on adsorbent products showed considerable variations of regression coefficient $R^2 = 0.9554$. However, the value of "n" falls within the feasibility limit showing positive signs of the adsorption process. In comparison of Langmuir and Freundlich isotherm models for the present scenario, Langmuir shows better fit compared to Freundlich confirming the sorption process if monolayer.

4.2. Toth isotherm model

Toth isotherm is a three-parameter isotherm, using an empirical modification of the Langmuir isotherm model in order to better approximate experimental data. The Toth isotherm shares the same general assumptions as the Freundlich isotherm model, which applies to heterogeneous adsorption systems that meet the low- and high-end bounds of adsorbate concentrations. The model is described as follows:

$$\text{TothIsothermmodel}\,\frac{q_e}{q_m} = \frac{K_e C_e}{\left[1 + (K_L C_e)^n\right]^{1/n}} \quad (5)$$

Where K_L is the Toth isotherm constant (mg/g) and n is the Toth adsorption intensity. In case of n = 1, the equation reduces to the Langmuir model supporting the monolayer adsorption phenomenon or else satisfies the multilayer heterogeneous adsorption reaction. In the present study of Cr (VI), Pb (II) adsorption onto HS, HS-IL the value of n is close to 1 with a regression coefficient of 0.9989 (see Fig. 11; Table 1), strongly confirms the adsorption mechanism is monolayer following the Langmuir isotherm model.

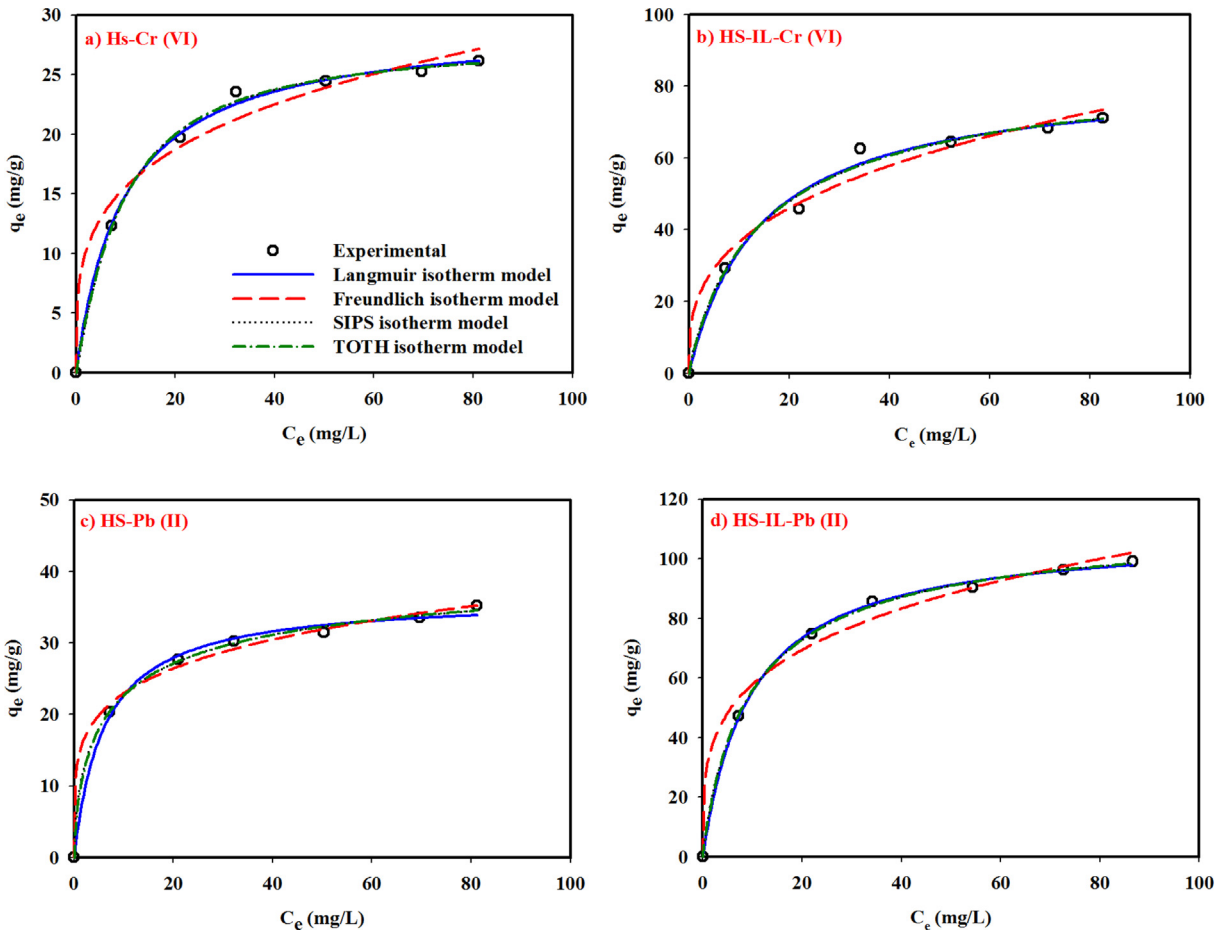

Fig. 11. Non-linear adsorption isotherm model studies with varied metal ions concentration a, b) Cr (VI) using HS, HS-IL; c, d) Pb (II) using HS, HS-IL.

Table 1
Equilibrium modeling data for the removal of Cr (VI), Pb (II) using HS, and HS-IL.

Material	Isotherm	Parameters	Cr (VI) Value	R^2	Pb (II) Value	R^2
HS	Langmuir	q_m (mg/g)	29.241	0.9973	36.382	0.9960
		K_L (L/mg)	0.1041		0.1649	
	Freundlich	K_f (mg/g)	8.469	0.9783	14.300	0.9694
		n	3.774		4.8789	
	SIPS	K_s	2.2805	0.9978	11.426	0.9983
		a	0.0812		0.2664	
		b	1.1406		0.6227	
	Toth	a	27.835	0.9989	44.670	0.9971
		b	0.0884		0.5371	
		n	0.8181		1.9367	
HS + IL	Langmuir	q_m (mg/g)	82.889	0.9901	108.631	0.9991
		K_L (L/mg)	0.0698		0.1044	
	Freundlich	K_f (mg/g)	17.109	0.9791	31.565	0.9772
		n	3.0289		3.8017	
	SIPS	K_s	7.1412	0.9903	13.7213	0.9928
		a	0.0818		0.1218	
		b	0.9010		0.9041	
	Toth	a	87.8568	0.9902	113.657	0.9931
		b	0.0779		0.1214	
		n	1.1614		1.1624	

4.3. Sips isotherm model

This isotherm model combines the Langmuir and Freundlich expressions and is typically used to determine the heterogeneity of the adsorption system. Further, the Sips isotherm model overcomes the Freundlich isotherm deficiencies of increased adsorption with the concentration. Another similarity is Sips resembles like Freundlich isotherm, but has a finite limit in case of higher concentrations. The non-linear form of Sips isotherm model equation is as follows.

$$\text{SipsIsothermmodel} q_e = \frac{q_m K_s C_e^m}{1 + K_s C_e^m} \quad (6)$$

The equilibrium concertation of adsorbate, maximum adsorption capacity, equilibrium constant, and Sips exponents were represented by C_e (mg/L), q_m (mg/g), K_s (L/mg), and m respectively. In the present study of Cr (VI), Pb (II) adsorption onto HS, HS-IL the value of n is close to 1 with a regression coefficient R^2 0.9989 (see Fig. 11; Table 1), strongly confirms the adsorption mechanism is monolayer following the Langmuir isotherm model.

Summarizing the comparative analysis of experimental adsorption with the theoretical expressions, the adsorption of the metal ions Cr (VI), Pb (II) strongly favors the monolayer and homogeneous adsorption phenomenon onto HS, HS-IL (Langmuir) having a better fit, regression coefficients over the other two isotherm models. Further, a comparative summary of the literature pertaining the separation of Cr (VI), and Pb (II) using various adsorbents are presented in Table 2.

Table 2
Summary of the literature pertaining the separation of Cr (VI), Pb (II).

Adsorbent	pH	Adsorption capacity (mg/g)	Reference
Cr (VI)			
Graphene oxide-dicationic ionic liquid composite	3	271.08	[60]
Ionic liquid immobilized cellulose	2	181.81	[61]
Ionic liquid impregnated sulphate-cross linked chitosan	3	250.90	[62]
Surface functionalized silica nanoparticles with poly(ionic liquids)	4	205.30	[63]
Ionic liquid grafted polyamide 6 (IL-g-PA6)	4	68.40	[64]
Hazel Sterculia Foetida L. (HS)	3	29.24	Present
HS-IL	3	82.88	
Pb (II)			
Alginate/chitosan (ALG/CHT) and alginate/N,N-dimethyl chitosan (ALG/DMC) polyelectrolyte complex (PEC)	5	560.20	[65]
Ionic liquid assisted mesoporous silica-graphene oxide nanocomposite	5	527.00	[66]
Hydrophobic Brønsted acidic amide-type ionic liquid	5	327.90	[67]
Thiopropyl-containing ionic liquid based periodic mesoporous organosilica	6	105.26	[68]
N,N-dimethyl chitosan/alginate-based adsorbents	5	560.20	[65]
Hazel Sterculia Foetida L. (HS)	5	36.38	Present
HS-IL	5	108.63	

4.4. Adsorption kinetics

Adsorption mechanism elucidates the reaction pathways, and the mechanism of solute adsorption onto the solid surface. The reaction mechanism, rate of reaction and other essential parametric evaluation is not possible by the solid–liquid equilibrium. Further, establishment of equilibrium elucidates the transfer mechanism of the solute across the boundary among two phases. However, the transfer of solute depends on the physico-chemical characteristics of the solid sorbent molecule, and the solution parting coefficient between bulk liquid and solid adsorbent determine its efficacy. Adsorption kinetic studies help to assess the above prospects in conjunction with the retention time, sorption rate and potential adsorption rate limiting step. Thus, this study covers three major kinetic models: pseudo-first-order (PFO) [50], pseudo-second-order (PSO) [51], Elovich models [52] in the formulation of the adsorption mechanism of Cr(VI), Pb (II) in the IL (BMIM-TFSI) functionalized HS seed powder. The temperature dependent sorption kinetics were solved by the following non-linear model equations listed below:

$$\text{PFOkinetics} : q_t = q_{e1}(1 - \exp(-k_1 t)) \quad (7)$$

$$\text{PSOkinetics} : q_t = \frac{q_{e2}^2 k_2 t}{1 + q_{e2} k_2 t} \quad (8)$$

$$\text{Non} - \text{linearElovich} q_t = \frac{1}{\beta} \ln(1 + \alpha\beta t) \quad (9)$$

The variables q_e (mg/g), q_t (mg/g) were the adsorptive capacities of Cr (VI), Pb (II) towards HS, HS-IL at time t, and equilibrium. k_1 (min^{-1}), k_2 (g/mg/min) are the PFO, PSO's rate constants. α (mg/g/min), β (g/mg) are the rate of adsorption desorption constants respectively.

Further, the experimental data was fitted to the corresponding plots of q_e vs T for Cr (VI) adsorbed onto HS, HS-IL Fig. 12 (a–f), Pb (II) onto HS, HS-IL Fig. 12 (g–l) resulted $q_{e,cal}$, k_1,k_2, α, βand the detailed summary of the values are shown in Table 3. As shown in the table the PSO kinetic model provided a good value of R^2 = 0.9985, with $q_{e,cal}$ = 26.0 (mg/g) for HS, 68.2 (mg/g) in case of HS-IL at 303 K. Similar trends were observed in case of Pb (II) favoring PSO with $q_{e,cal}$ = 37.8 (mg/g) for HS, 87.1 (mg/g) in case of HS-IL at 303 K. These calculated adsorption values were in close proximity with the actual experimental observations. This trend of adsorption leaning towards the PSO suggests chemical adsorption or chemisorption is the rate limiting step. Besides, Elovich kinetic model confirms the chemisorptive behavior by an assumption of solid systems were heterogeneous in nature [6]. From Table 3 the increasing values of α, and the decreasing values of β suggesting the exchange or sharing of electrons between sorbate and sorbent molecules via valence forces, thus confirming the chemisorption is the rate limiting step [53]. Summarizing the kinetic studies, the key observations are PSO is a better fit

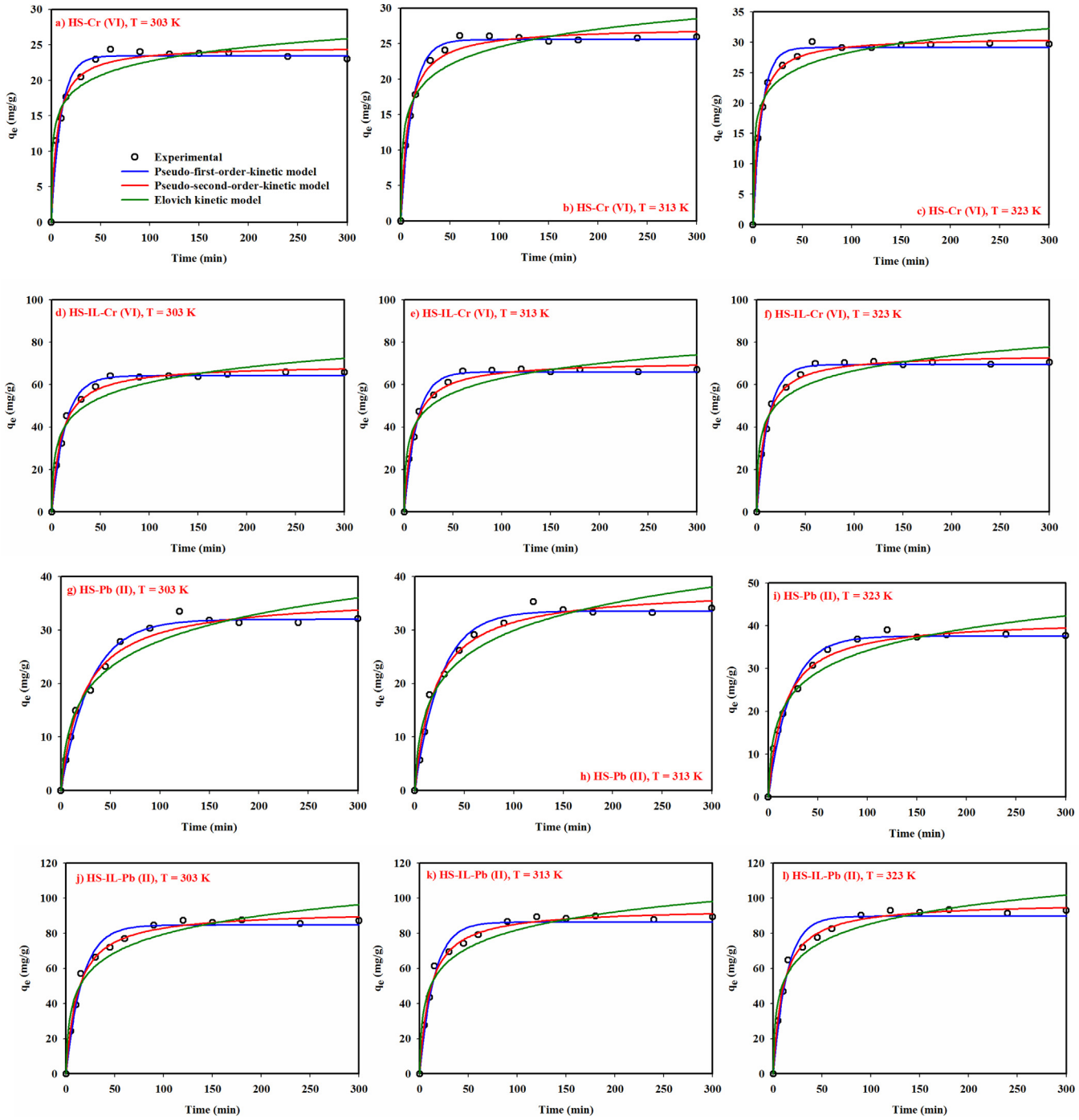

Fig. 12. Nonlinear kinetic studies on separating (a-f) Cr (VI), (g-l) Pb (II) using HS, HS-IL.

Table 3
Kinetic modeling of data for the separation of Cr (VI), Pb (II) using HS, HS-IL.

Adsorbate	T (K)	Pseudo-first order kinetic model				Pseudo-second order kinetic model			Elovich kinetic model		
		$q_{e,\ exp}$ (mg/g)	$q_{e1,\ cal}$ (mg/g)	k_1 (1/min)	R^2	$q_{e2,\ cal}$ (mg/g)	k_2 (g/mg min)	R^2	α (mg/g/min)	β (g/mg)	R^2
Cr (VI)											
HS	303	25.53	23.42	0.1023	0.9827	26.01	0.0063	0.9909	3.38	0.0940	0.3484
	313	27.50	25.55	0.0860	0.9815	26.97	0.0067	0.9912	7.60	0.0632	0.9068
	323	31.06	29.12	0.1131	0.9883	30.83	0.0059	0.9944	12.91	0.0274	0.9562
HS + IL	303	67.92	64.18	0.7322	0.9737	68.19	0.0015	0.9906	27.29	0.0965	0.9407
	313	71.27	65.97	0.0789	0.9856	71.02	0.0017	0.9950	44.61	0.0820	0.9427
	323	75.09	69.41	0.0839	0.9802	74.52	0.0016	0.9915	52.64	0.5105	0.9133
Pb (II)											
HS	303	37.01	31.97	0.0335	0.9258	37.81	0.0013	0.9952	8.60	0.065	0.9123
	313	38.26	33.54	0.0382	0.9414	39.43	0.0049	0.9947	19.02	0.047	0.9472
	323	41.54	37.54	0.0453	0.9526	41.54	0.0015	0.9911	25.86	0.024	0.9704
HS + IL	303	91.17	84.64	0.0606	0.9252	92.89	0.0009	0.9918	24.05	0.134	0.9181
	313	93.95	86.32	0.0683	0.9105	94.24	0.0010	0.9968	32.17	0.112	0.9062
	323	97.86	89.80	0.0719	0.9111	97.61	0.0008	0.9923	47.50	0.095	0.9354

compared to PFO with better R^2 in the both the cases of Cr (VI), Pb (II) adsorption onto HS, HS-IL. And through Elovich kinetic model, the chemisorption behavior is the rate limiting step.

4.5. Adsorption thermodynamics

According to the fundamental principles of thermodynamics, for an isolated system the total energy of the system remains conserved and the entropy changes for all irreversible reactions are continuously increasing. Thus, the influence of the reaction temperature is highly important to estimate the adsorption phenomenon. Hence, a series of series were conducted on the adsorption process of the Cr (VI), Pb (II) onto the surface of HS, HS-IL adsorbents at variable temperatures of 303–323 K, maintaining the other adsorption variables at optimal conditions. Fig. 13a describes the increasing tendency of the adsorption capacity with respect to increase in temperature signifies the increasing temperature chemically changes the adsorbent, adsorption sites and activity. This means that the spread of sorbate molecules has been altered by the temperature influence, resulting in an increase in the mass transfer rate from the volume of the molecules to the limit layer at the surface of the sorbent molecules [54]. Furthermore, increasing temperature favors intermolecular forces between the adsorbed and adsorbed molecules, testing for greater mobility towards the adsorbing surface. Other temperature related studies such as evaluating the Gibbs free energy change, enthalpy, and entropy determines the feasibility, spontaneity, and heat change for the biosorption process. The mathematic expressions for these thermodynamic parameters are as follows:

$$\Delta G^0 = -RT\ln K_c \tag{10}$$

$$K_c = \frac{C_{Ae}}{C_e} \tag{11}$$

$$\Delta G^0 = \Delta H^0 - T\Delta S^0 \tag{12}$$

$$\ln K_c = -\frac{\Delta G^0}{RT} = -\frac{\Delta H^0}{RT} + \frac{\Delta S^0}{R} \tag{13}$$

From these expressions, the variables R, T, K_c, C_{Ae}, C_e, are known to be universal gas constant (J/mol K), absolute temperature (K), distribution coefficient, equilibrium concentrations (mg/L) of Cr (VI), Pb (II) on sorbent HS, HS-IL respectively. The thermodynamic parameters ΔG^0, ΔH^0, ΔS^0 were calculated from the plot of ln K_c and I/T as slope and intercept (Fig. 13b). A detailed summary of the calculated thermodynamic parameters is presented in Table 4. From Table, the negative value of the ΔG^0 in the temperature range

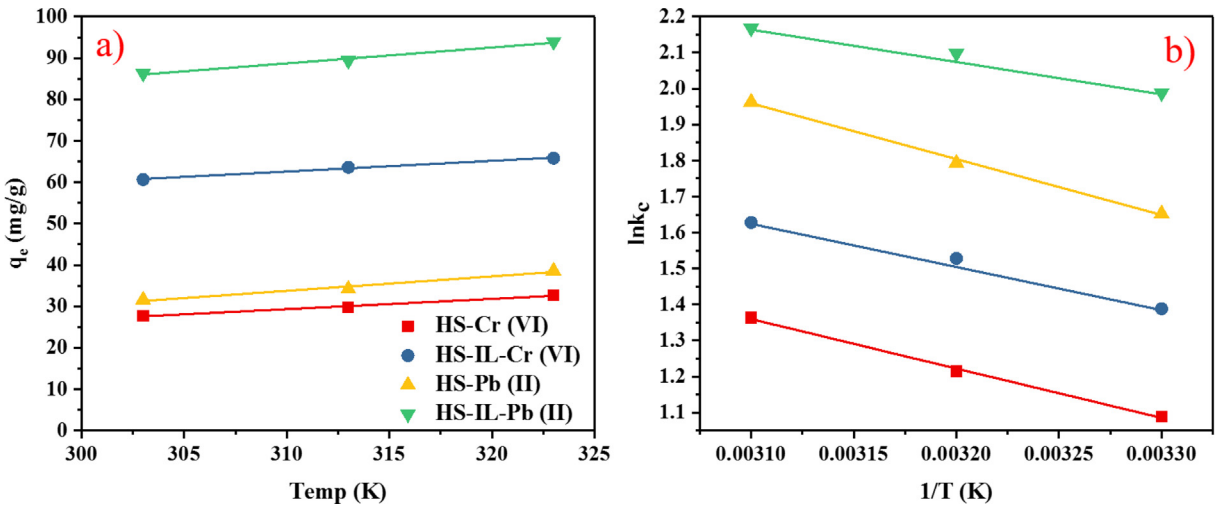

Fig. 13. a) Thermodynamic studies on the adsorption of Cr (VI), Pb (II) metal ions onto HS, HS-IL, b) Van't Hoff plot for the adsorption of Cr (VI), Pb (II) onto HS, HS-IL.

Table 4
Thermodynamic assessment on adsorption of Cr (VI), Pb (II) onto HS, HS-IL.

Adsorbate	T (K)	ΔG^o (kJ/mol)	ΔH^o (kJ/mol)	ΔS^o (J/mol K)
HS-Cr (VI)	303	−2.7429	11.16	22.14
	313	−3.0770		
	323	−3.4344		
HS-IL-Cr (VI)	303	−3.2540	10.07	22.51
	313	−3.6183		
	323	−3.8769		
HS-Pb (II)	303	−2.4601	12.64	22.95
	313	−2.8020		
	323	−3.2448		
HS-IL-Pb (II)	303	−2.8500	7.37	18.06
	313	−3.1463		
	323	−3.3058		

of (303–313 K) tends to increase linearly signifies the spontaneity of the reaction and adsorption is feasible thermodynamically. Further, the positive value of enthalpy change ΔH^0 for the above mentioned temperature range confirms the endothermic nature of the reaction [55]. The positive value of entropy change ΔS^0 explains that the solid/solution interface randomness is increasing in the sorption mechanism [56]. Another critical outcome of the study that can be confirmed through the magnitude of the enthalpy change is the nature of adsorption i.e., either physiosorption or chemisorption. In case of physiosorption, the energy requirements are meagreΔH^0 < 1 (K cal/mol); and hence the attainment of equilibrium is very rapid and easy. In general, chemisorption demands higher energies usuallyΔH^0 > 5 (K cal/mol) [57], and the attainment of equilibrium is feasible at higher enthalpy values.

4.6. Desorption studies

To scale up the adsorption process and the design parameters, it is highly important to evaluate the reusability and the regeneration tendency of the adsorbent materials. Therefore, the regeneration property of the HS, HS-IL was studied through sorption–desorption studies. The adsorption tests were performed by considering 30 mL of 300 ppm Cr (VI), Pb (II) solutions separately, adding 0.1 g, 0.4 g of HS, HS-IL to Cr (VI), and Pb (II) respectively. The solution pH was maintained optimal (pH = 3, 5 for Cr (VI), PB (II)) at 303 K, under agitation of 200, 300 rpm respectively for 90 and 180 min. Later the solution of was dried in a furnace at 333 K for 8 h, sediment was recovered to perform the desorption studies. Various eluents were selected comprising acidic (0.1 M HCl, 0.1 M HNO_3), alkaline (0.1 M NaOH, 0.1 M KOH), H_2O, and organic solvents (100 % CH_3OH, 100% C_2H_5OH) to test the suitability of the recovery medium. From Fig. 14 it is evident that the maximum recovery of the sorbent HS, HS-IL from the metal ion solution Cr (VI), was achieved through NaOH, and HCl in case of Pb (II), reporting a maximum recovery of 66.5% (Cr (VI) with HS), 89.2% (Cr (VI) with HS-IL), 69.5% (Pb (II) with HS), 89.6% ((Pb (II) with HS-IL)) respectively. This shows that raw HS recovery mostly favors the acidic medium whereas the IL functionalized HS favors the alkaline medium. The reason ascribed to the higher recovery in alkaline medium is due to the interaction among the hydroxyl groups and the adsorbent surface. Further, the bio sorbent surface acquires negative charge and electrostatic repulsion with metal ions (Cr VI) tends to detach the adsorbent molecule [58]. On the other hand, ion exchange type interactions are attributed to the affinity of the acidic medium as an eluent in cases of Pb (II) instead of to chemical sorption. Furthermore, the hydroxyl and carboxylic groups of the HS rendered acid solutions easier to desorb and regenerate [59]. Thus, 0.1 M NaOH is considered as a suitable eluent in recovering HS, HS-IL from the Cr (VI) solution, 0.1 M HCL showed better desorption of HS, HS-IL from Pb (II).

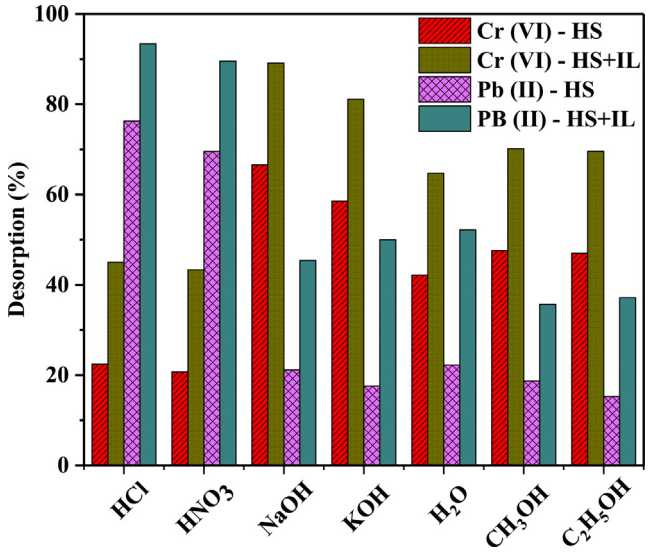

Fig. 14. Effect of eluents on the desorption of HS, HS-IL from Cr (VI), Pb (II) metal ion solutions.

4.7. Regeneration studies

The performance of the adsorbent and its reuse is a primitive indicator in evaluating the viability of the adsorbent for a specific adsorption process. The more the reusability, the more the commercial importance, and thus it is mandate to evaluate the adsorption–desorption cycles in the adsorption mechanism. In the present study, the adsorption–desorption experiments were performed on a successive note using the optimal eluents to recover HS, HS-IL from Pb (II), and NaOH for Cr (VI) solutions respectively. Fig. 15 represents the clear picture on the ability of the adsorbent tested over successive cycles of the adsorption–desorption phenomenon. From the figure it can be seen that the ability of the adsorbent is limited and effective till two cycles; adsorption (31.5%–22.5%), desorption (75.9%–51.2%) for HS, adsorption (64.3%–53.5%), desorption (81.3% −64.1%) for HS-IL in case of Cr (VI), and declined rapidly thereafter. Whereas, the adsorbent HS seems promising up to five consecutive cycles of adsorption (30.4%–13.6%), desorption (81.5%–56.3%), and for HS-IL it was; adsorption (86.3%–59.7%), desorption (92.3%–66.3%) in case of Pb (II). In summary, the adsorbent reuse was successful for three

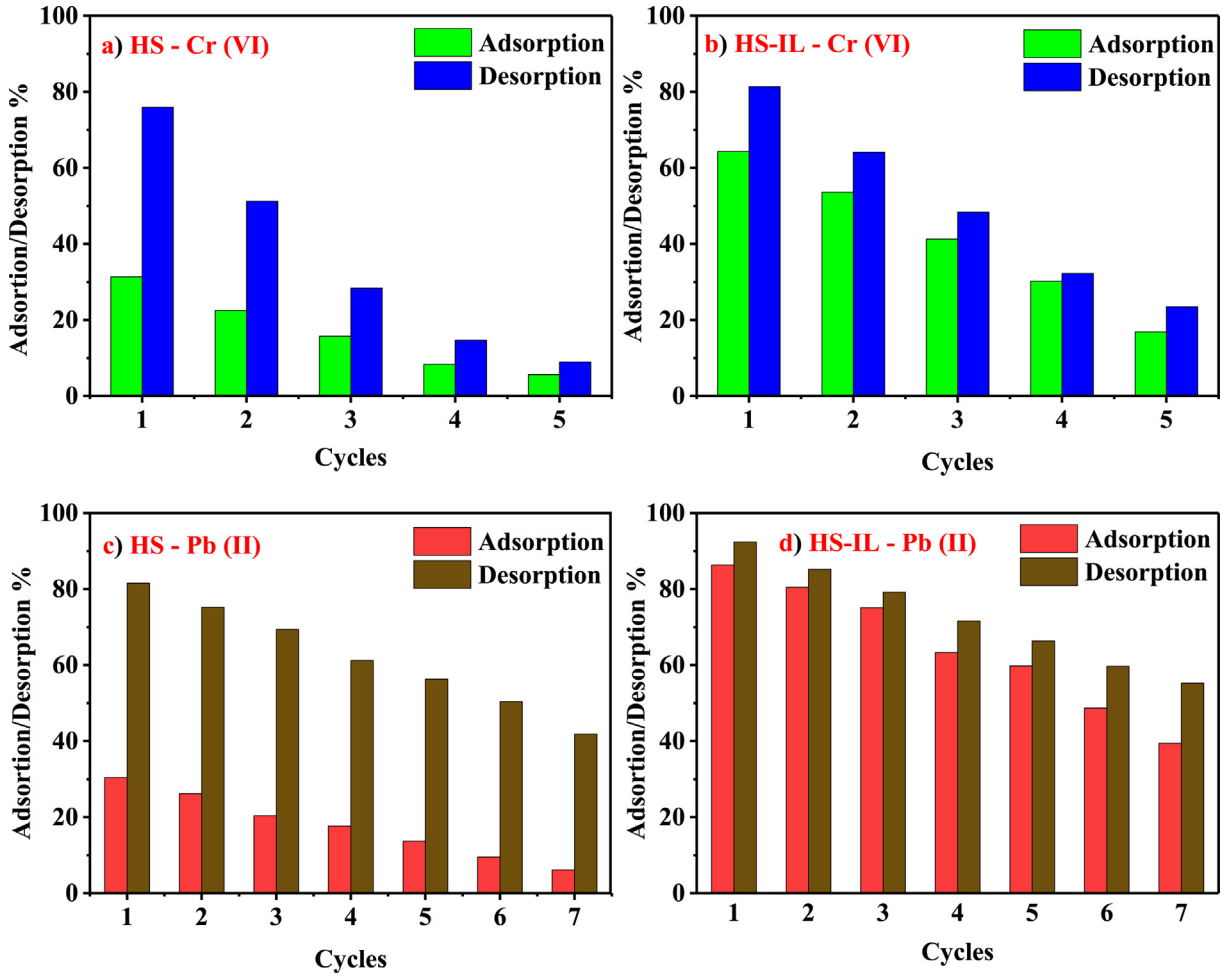

Fig. 15. Reusability studies on the adsorbent HS, HS-IL for the separation of Cr (VI), Pb (II).

cycles in Cr (VI), whereas it can be used up to six consecutive times to extract from Pb (II) solutions.

5. Conclusions

The production and characterisation of a HAZEL Sterculia Foetida L. adsorbent material functionalized with 1-butyl-3-methylimidazolium bis (trifluoromethyl sulfonyl) imide were described in detail in this paper. the adsorbent was evaluated for its ability to separate metal ions such as Cr (VI) and Pb (II) from an aquatic effluent stream. Various isotherm models were tested, and the results indicate that an adsorption process is sufficient for removing heavy metals from the environment. Through kinetic modeling, it was determined that the adsorption phenomena followed pseudo-second order kinetics as a result of monolayer adsorption with chemisorption, as confirmed by the Elovich model. In terms of thermodynamics, the adsorption phenomenon is endothermic and impulsive in character. Finally, regeneration tests were conducted and it was determined that, in comparison to traditional adsorbents, ionic liquid functionalized sorbents have a greater capacity for reuse. The adsorption and desorption cycles demonstrated a six-fold reusability of the same adsorbent, a very cost-effective property. Finally, the natural biomass waste as synthesized and functionalized with green solvents poses no damage to the ecology, but rather provides significant benefits by separating complicated divalent lead and hexavalent chromium from aqueous steams.

CRediT authorship contribution statement

Anjani R.K. Gollakota: Conceptualization, Methodology, Writing – original draft, Formal analysis, Writing – review & editing. **Venkata Subbaiah Munagapati:** Conceptualization, Data curation. **Chi-Min Shu:** Supervision, Conceptualization, Resources, Writing – review & editing, Validation. **Jet-Chau Wen:** Writing – review & editing, Validation.

Declaration of Competing Interest

The authors declare that they have no known competing financial interests or personal relationships that could have appeared to influence the work reported in this paper.

Acknowledgements

The authors greatly acknowledge the cooperation and support of PS&DPL team.

References

[1] A.R.K. Gollakota, V.S. Munagapati, S. Gautam, J.-C. Wen, C.-M. Shu, Hydrothermal tuning of morphology of aluminophosphate (AlPO-14) framework for the adsorption of Rhodamine 6G dye, Adv. Powder Technol. 32 (8) (2021) 3002–3015, https://doi.org/10.1016/j.apt.2021.06.015.
[2] A.R.K. Gollakota, V.S. Munagapati, K.P. Shadangi, G.M. Reddy, J.-C. Wen, C.-M. Shu, Encapsulating toxic Rhodamine 6G dye, and Cr (VI) metal ions from liquid

phase using AlPO4-5 molecular sieves. Preparation, characterization, and adsorption parameters, J. Mol. Liq. 336 (2021) 116549, https://doi.org/10.1016/j.molliq.2021.116549.
[3] Y.A.B. Neolaka, Y. Lawa, J.N. Naat, A.A. Pau Riwu, H. Darmokoesoemo, G. Supriyanto, C.I. Holdsworth, A.N. Amenaghawon, H.S. Kusuma, A Cr(VI)-imprinted-poly(4-VP-co-EGDMA) sorbent prepared using precipitation polymerization and its application for selective adsorptive removal and solid phase extraction of Cr(VI) ions from electroplating industrial wastewater, React. Funct. Polym. 147 (2020) 104451, https://doi.org/10.1016/j.reactfunctpolym.2019.104451.
[4] Y.A.B. Neolaka, Y. Lawa, J. Naat, A.A.P. Riwu, Y.E. Lindu, H. Darmokoesoemo, B. A. Widyaningrum, M. Iqbal, H.S. Kusuma, Evaluation of magnetic material IIP@GO-Fe3O4 based on Kesambi wood (Schleichera oleosa) as a potential adsorbent for the removal of Cr(VI) from aqueous solutions, React. Funct. Polym. 166 (2021) 105000, https://doi.org/10.1016/j.reactfunctpolym.2021.105000.
[5] Y.A.B. Neolaka, G. Supriyanto, H.S. Kusuma, Adsorption performance of Cr(VI)-imprinted poly(4-VP-co-MMA) supported on activated Indonesia (Ende-Flores) natural zeolite structure for Cr(VI) removal from aqueous solution, J. Environ. Chem. Eng. 6 (2) (2018) 3436–3443.
[6] A.R.K. Gollakota, V.S. Munagapati, V. Volli, S. Gautam, J.-C. Wen, C.-M. Shu, Coal bottom ash derived zeolite (SSZ-13) for the sorption of synthetic anion Alizarin Red S (ARS) dye, J. Hazard. Mater. 416 (2021) 125925, https://doi.org/10.1016/j.jhazmat.2021.125925.
[7] E.P. Kuncoro, T. Soedarti, T.W.C. Putranto, H. Darmokoesoemo, N.R. Abadi, H.S. Kusuma, Characterization of a mixture of algae waste-bentonite used as adsorbent for the removal of Pb2+ from aqueous solution, Data Br. 16 (2018) 908–913, https://doi.org/10.1016/j.dib.2017.12.030.
[8] M. Qasemi, M. Afsharnia, A. Zarei, A.A. Najafpoor, S. Salari, M. Shams, Phenol removal from aqueous solution using Citrullus colocynthis waste ash, Data Br. 18 (2018) 620–628, https://doi.org/10.1016/j.dib.2018.03.049.
[9] B. Ekka, L. Rout, M.K. Sahu Aniket Kumar, R.K. Patel, P. Dash, Removal efficiency of Pb(II) from aqueous solution by 1-alkyl-3-methylimidazolium bromide ionic liquid mediated mesoporous silica, J. Environ Chem. Eng. 3 (2) (2015) 1356–1364.
[10] T. Ajioka, S. Oshima, N. Hirayama, Use of 8-sulfonamidoquinoline derivatives as chelate extraction reagents in ionic liquid extraction system, Talanta. 74 (4) (2008) 903–908, https://doi.org/10.1016/j.talanta.2007.07.020.
[11] H. Luo, S. Dai, P.V. Bonnesen, A.C. Buchanan, J.D. Holbrey, N.J. Bridges, R.D. Rogers, Extraction of cesium ions from aqueous solutions using calix[4]arene-bis(tert.octylbenzo-crown-6) in ionic liquids, Anal. Chem. 76 (11) (2004) 3078–3083, https://doi.org/10.1021/ac049949k10.1021/ac049949k.s001.
[12] H. Heitzman, B. Young, D. Rausch, P. Rickert, D. Stepinski, M. Dietz, Fluorous ionic liquids as solvents for the liquid-liquid extraction of metal ions by macrocyclic polyethers, Talanta. 69 (2) (2006) 527–531, https://doi.org/10.1016/j.talanta.2005.09.046.
[13] K. Shimojo, M. Goto, Solvent extraction and stripping of silver ions in room-temperature ionic liquids containing calixarenes, Anal. Chem. 76 (17) (2004) 5039–5044, https://doi.org/10.1021/ac049549x.
[14] S. Pandey, Analytical applications of room-temperature ionic liquids: A review of recent efforts, Anal. Chim. Acta. 556 (1) (2006) 38–45, https://doi.org/10.1016/j.aca.2005.06.038.
[15] G.-T. Wei, Z. Yang, C.-J. Chen, Room temperature ionic liquid as a novel medium for liquid/liquid extraction of metal ions, Anal. Chim. Acta. 488 (2) (2003) 183–192, https://doi.org/10.1016/S0003-2670(03)00660-3.
[16] M.T. Friend, T.G. Parker, T. Mastren, V. Mocko, M. Brugh, E.R. Birnbaum, M.E. Fassbender, Extraction chromatography of 225Ac and lanthanides on N, N-dioctyldiglycolamic acid /1-butyl-3-methylimidazolium bis (trifluoromethylsulfonyl)imide solvent impregnated resin, J. Chromatogr. A. 1624 (2020) 461219, https://doi.org/10.1016/j.chroma.2020.461219.
[17] X. Zheng, K. Fukuhara, Y. Hijikata, J. Pirillo, H. Sato, K. Takahashi, S. ichiroNoro, T. Nakamura, Understanding the interactions between the bis (trifluoromethylsulfonyl)imide anion and absorbed CO2 using X-ray diffraction analysis of a soft crystal surrogate, Commun. Chem. 3 (2020) 1–7, https://doi.org/10.1038/s42004-020-00390-1.
[18] L.-Q. Jiang, Z. Fang, X.-K. Li, J. Luo, Production of 2,3-butanediol from cellulose and Jatropha hulls after ionic liquid pretreatment and dilute-acid hydrolysis, AMB Express. 3 (1) (2013), https://doi.org/10.1186/2191-0855-3-48.
[19] S.H. Mnyipika, T.S. Munonde, P.N. Nomngongo, Mno2 @reduced graphene oxide nanocomposite-based electrochemical sensor for the simultaneous determination of trace cd(Ii), zn(ii) and cu(ii) in water samples, Membranes (Basel). 11 (7) (2021) 517, https://doi.org/10.3390/membranes11070517.
[20] M.R.N. Nabilah, M.A. Alwi, M.S. Su'ait, M. Imperiyka, S.A. Hanifah, A. Ahmad, N. H. Hassan, M.Y.A. Rahman, Effect of ionic liquid 1-butyl-3-methylimidazolium bis(trifluoromethanesulfonyl)imide on the properties of poly(glycidyl methacrylate) based solid polymer electrolytes, Russ. J. Electrochem. 52 (4) (2016) 362–373, https://doi.org/10.1134/S1023193516040091.
[21] S. Lowell, J.E. Shields, Adsorption isotherms, Powder Surf, Area Porosity. (1991) 11–13, https://doi.org/10.1007/978-94-015-7955-1_3.
[22] X. Li, K. Xu, Y. Zhang, C. Sun, Y. He, S. Amancio, Optical determination of lead chrome green in green tea by Fourier transform infrared (FT-IR) transmission spectroscopy, PLoS One. 12 (1) (2017) e0169430, https://doi.org/10.1371/journal.pone.0169430.
[23] K. Yuniarto, Y.A. Purwanto, S. Purwanto, B.A. Welt, H.K. Purwadaria, T.C. Sunarti, Infrared and Raman studies on polylactide acid and polyethylene glycol-400 blend, AIP Conf. Proc. 1725 (2016), https://doi.org/10.1063/1.4945555.
[24] A.M. Abdul-Munaim, T. Holland, P. Sivakumar, D.G. Watson, Absorption wavebands for discriminating oxidation time of engine oil as detected by FT-IR spectroscopy, Lubricants. 7 (2019) 22–25, https://doi.org/10.3390/lubricants7030024.
[25] P. Senthil Kumar, C. Senthamarai, A.S.L. Sai Deepthi, R. Bharani, Adsorption isotherms, kinetics and mechanism of Pb(II) ions removal from aqueous solution using chemically modified agricultural waste, Can. J. Chem. Eng. 91 (12) (2013) 1950–1956.
[26] Y. Yin, H. Yin, Z. Wu, C. Qi, H. Tian, W. Zhang, Z. Hu, L. Feng, Characterization of coals and coal ashes with high Si content using combined second-derivative infrared spectroscopy and Raman spectroscopy, Crystals. 9 (2019), https://doi.org/10.3390/cryst9100513.
[27] T. Yamada, M. Mizuno, Characteristic Spectroscopic Features because of Cation-Anion Interactions Observed in the 700–950 cm-1 Range of Infrared Spectroscopy for Various Imidazolium-Based Ionic Liquids, ACS Omega. 3 (7) (2018) 8027–8035, https://doi.org/10.1021/acsomega.8b0093810.1021/acsomega.8b00938.s001.
[28] A. Shirani, J. Lee, D. Berman, Thermal stability and gas absorption characteristics of ionic liquid-based solid polymer electrolytes, J. Chem. Phys. 154 (5) (2021) 054902, https://doi.org/10.1063/5.0037978.
[29] H. Huang, Y. Yang, J. Chang, C. Su, An Ether Bridge between Cations to Extend the Applicability of ionic liquids in electric double layer capacitors, J. Mater. Chem. A. 2 (2016) 1–13.
[30] F. Shi, Y. Deng, Abnormal FT-IR and FTRaman spectra of ionic liquids confined in nano-porous silica gel, Spectrochim. Acta - Part A Mol. Biomol. Spectrosc. 62 (1-3) (2005) 239–244, https://doi.org/10.1016/j.saa.2004.12.031.
[31] S. Mazurek, A. Mucciolo, B.M. Humbel, C. Nawrath, Transmission Fourier transform infrared microspectroscopy allows simultaneous assessment of cutin and cell-wall polysaccharides of Arabidopsis petals, Plant J. 74 (5) (2013) 880–891, https://doi.org/10.1111/tpj.12164.
[32] C. Roth, S. Chatzipapadopoulos, D. Kerlé, F. Friedriszik, M. Lütgens, S. Lochbrunner, O. Kühn, R. Ludwig, Hydrogen bonding in ionic liquids probed by linear and nonlinear vibrational spectroscopy, New J. Phys. 14 (10) (2012) 105026, https://doi.org/10.1088/1367-2630/14/10/105026.
[33] A.M. Elbarbary, Y.H. Gad, Radiation Synthesis and Characterization of Poly (vinyl alcohol)/acrylamide/TiO2/SiO2 Nanocomposite for Removal of Metal Ion and Dye from Wastewater, J. Inorg. Organomet. Polym. Mater. 31 (10) (2021) 4103–4125, https://doi.org/10.1007/s10904-021-02029-7.
[34] A. Nasrollahpour, S.E. Moradi, Hexavalent chromium removal from water by ionic liquid modified metal-organic frameworks adsorbent, Microporous Mesoporous Mater. 243 (2017) 47–55, https://doi.org/10.1016/j.micromeso.2017.02.006.
[35] S. Saleem, A.N.S. Saqib, A. Mujahid, M. Hanif, G. Mustafa, T. Mahmood, A. Waseem, A.R. Khan, Extraction of Pb(II) from water samples by ionic liquid-modified silica sorbents, Desalin. Water Treat. 52 (40-42) (2014) 7915–7924, https://doi.org/10.1080/19443994.2014.922497.
[36] D.Corporation, The framework topology of Z S M - 2 2 : A high silica zeolite, 5 (1985) 349–351.
[37] M. Rao, A.V. Parwate, A.G. Bhole, Removal of Cr6+ and Ni2+ from aqueous solution using bagasse and fly ash, Waste Manag. 22 (7) (2002) 821–830, https://doi.org/10.1016/S0956-053X(02)00011-9.
[38] R. Labied, O. Benturki, A.Y. Eddine Hamitouche, A. Donnot, Adsorption of hexavalent chromium by activated carbon obtained from a waste lignocellulosic material (Ziziphus jujuba cores): Kinetic, equilibrium, and thermodynamic study, Adsorpt. Sci. Technol. 36 (3-4) (2018) 1066–1099, https://doi.org/10.1177/0263617417750739.
[39] L. Sun, M. Wang, W. Li, S. Luo, Y. Wu, C. Ma, S. Liu, Adsorption separation of Cr (VI) from a water phase using multiwalled carbon nanotube-immobilized ionic liquids, ACS Omega. 5 (36) (2020) 22827–22839, https://doi.org/10.1021/acsomega.0c0201610.1021/acsomega.0c02016.s001.
[40] Y. Zhang, Y. Cao, H. Wang, Multi-Interactions in Ionic Liquids for Natural Product Extraction, Molecules. 26 (2020) 1–18, https://doi.org/10.3390/molecules26010098.
[41] J.H. Waiter, Reverse engineering of bioadhesion in marine mussels, Ann. N. Y. Acad. Sci. 875 (1) (1999) 301–309, https://doi.org/10.1111/j.1749-6632.1999.tb08513.x.
[42] R.L. Davidovich, V. Stavila, D.V. Marinin, E.I. Voit, K.H. Whitmire, Stereochemistry of lead(II) complexes with oxygen donor ligands, Coord. Chem. Rev. 253 (9-10) (2009) 1316–1352, https://doi.org/10.1016/j.ccr.2008.09.003.
[43] M.Pooresmaeil, H.Namazi, Application of polysaccharide-based hydrogels for water treatments, Elsevier Inc., 2019. doi:10.1016/B978-0-12-816421-1.00014-8.
[44] L.i. Wang, J. Zhang, R. Zhao, C. Li, Y.e. Li, C. Zhang, Adsorption of basic dyes on activated carbon prepared from Polygonum orientale Linn: Equilibrium, kinetic and thermodynamic studies, Desalination. 254 (1-3) (2010) 68–74, https://doi.org/10.1016/j.desal.2009.12.012.
[45] M.E. Mahmoud, M.T.H. Abou Kana, A.A. Hendy, Synthesis and implementation of nano-chitosan and its acetophenone derivative for enhanced removal of metals, Int. J. Biol. Macromol. 81 (2015) 672–680, https://doi.org/10.1016/j.ijbiomac.2015.08.063.
[46] A.R.K. Gollakota, V. Volli, V.S. Munagapati, J.-C. Wen, C.-M. Shu, Synthesis of novel ZSM-22 zeolite from Taiwanese coal fly ash for the selective separation

of Rhodamine 6G, J. Mater. Res. Technol. 9 (6) (2020) 15381–15393, https://doi.org/10.1016/j.jmrt.2020.10.070.
[47] V.R. Choudhary, D.B. Akolekar, A.P. Singh, S.D. Sansare, Sorption properties of crystalline molecular sieve AlPO4-5, J. Catal. 111 (1988) 23–40, https://doi.org/10.1016/0021-9517(88)90062-0.
[48] M.H. Armbruster, J.B. Austin, The Adsorption of Gases on Plane Surfaces of Mica, J. Am. Chem. Soc. 60 (2) (1938) 467–475, https://doi.org/10.1021/ja01269a066.
[49] F.r. Juretzka, Kolloidfiillung und Adsorption., Juretzka Gattierung von Zinkblende Und Galmei, [. 20 (18) (1907) 750–754, https://doi.org/10.1002/ange.19070201806.
[50] S. Lagergren, Zur theorie der sogenanntan adsorption gloster stoffe, K. Sven. Vetenskapsakademiens. Handl. 24 (1989) 1–39.
[51] Y.S. Ho, G. McKay, Pseudo-second order model for sorption processes, Process Biochem. 34 (1999) 451–465, https://doi.org/10.1021/acs.oprd.7b00090.
[52] H. Austin Taylor, N. Thon, Kinetics of Chemisorption, J. Am. Chem. Soc. 74 (1952) 4169–4173, https://doi.org/10.1021/ja01136a063.
[53] F. Gomri, G. Finqueneisel, T. Zimny, S.A. Korili, A. Gil, M. Boutahala, Adsorption of Rhodamine 6G and humic acids on composite bentonite–alginate in single and binary systems, Appl. Water Sci. 8 (6) (2018), https://doi.org/10.1007/s13201-018-0823-6.
[54] R.S. Blackburn, Natural polysaccharides and their interactions with dye molecules: Applications in effluent treatment, Environ. Sci. Technol. 38 (2004) 4905–4909, https://doi.org/10.1021/es049972n.
[55] Y. Zhou, Y. Min, H. Qiao, Q. Huang, E. Wang, T. Ma, Improved removal of malachite green from aqueous solution using chemically modified cellulose by anhydride, Int. J. Biol. Macromol. 74 (2015) 271–277, https://doi.org/10.1016/j.ijbiomac.2014.12.020.
[56] F. Batool, J. Akbar, S. Iqbal, S. Noreen, S.N.A. Bukhari, Study of Isothermal, Kinetic, and Thermodynamic Parameters for Adsorption of Cadmium: An Overview of Linear and Nonlinear Approach and Error Analysis, Bioinorg. Chem. Appl. 2018 (2018) 1–11, https://doi.org/10.1155/2018/3463724.
[57] D.Wu, T..McDonald, Z.Quan, S..Ushakov, P.Zhang, J..Long, A.Navrotsky, Thermodynamic Complexity of Carbon Capture in Alkylamine-Functionalized Metal-Organic Frameworks, J. Mater. Chem. A. 0 (6926) 1–7. doi:10.1039/x0xx00000x.
[58] K. Vijayaraghavan, J. Mao, Y.-S. Yun, Biosorption of methylene blue from aqueous solution using free and polysulfone-immobilized Corynebacterium glutamicum: Batch and column studies, Bioresour. Technol. 99 (8) (2008) 2864–2871, https://doi.org/10.1016/j.biortech.2007.06.008.
[59] J. Bayuo, K.B. Pelig-ba, M.A. Abukari, Optimization of Adsorption Parameters for Effective Removal of Lead (II) from Physical Chemistry : An Indian Journal Optimization of Adsorption Parameters for Effective Removal of Lead (II) from Aqueous Solution, Phys Chem Ind J. 14 (2019) 123.
[60] J. Shang, Y. Guo, D. He, W. Qu, Y. Tang, L. Zhou, R. Zhu, A novel graphene oxide-dicationic ionic liquid composite for Cr(VI) adsorption from aqueous solutions, J. Hazard. Mater. 416 (2021) 125706, https://doi.org/10.1016/j.jhazmat.2021.125706.
[61] Z. Dong, L. Zhao, Covalently bonded ionic liquid onto cellulose for fast adsorption and efficient separation of Cr(VI): Batch, column and mechanism investigation, Carbohydr. Polym. 189 (2018) 190–197, https://doi.org/10.1016/j.carbpol.2018.02.038.
[62] A. Shekhawat, S. Kahu, D. Saravanan, R. Jugade, Synergistic behaviour of ionic liquid impregnated sulphate-crosslinked chitosan towards adsorption of Cr (VI), Int. J. Biol. Macromol. 80 (2015) 615–626, https://doi.org/10.1016/j.ijbiomac.2015.07.035.
[63] G. Yang, Q. Huang, H. Huang, J. Chen, Y. Lei, F. Deng, M. Liu, Y. Wen, X. Zhang, Y. Wei, Preparation of cationic poly(ionic liquids) functionalization of silica nanoparticles via multicomponent condensation reaction with significant enhancement of adsorption capacity, J. Mol. Liq. 300 (2020) 112267, https://doi.org/10.1016/j.molliq.2019.112267.
[64] X. Zheng, F. Chen, X. Zhang, H. Zhang, Y. Li, J. Li, Ionic liquid grafted polyamide 6 as porous membrane materials: Enhanced water flux and heavy metal adsorption, Appl. Surf. Sci. 481 (2019) 1435–1441, https://doi.org/10.1016/j.apsusc.2019.03.111.
[65] K.B. Rufato, V.C. Almeida, M.J. Kipper, A.F. Rubira, A.F. Martins, E.C. Muniz, Polysaccharide-based adsorbents prepared in ionic liquid with high performance for removing Pb(II) from aqueous systems, Carbohydr. Polym. 215 (2019) 272–279, https://doi.org/10.1016/j.carbpol.2019.03.095.
[66] B. Barik, A. Kumar, P.S. Nayak, L.S.K. Achary, L. Rout, P. Dash, Ionic liquid assisted mesoporous silica-graphene oxide nanocomposite synthesis and its application for removal of heavy metal ions from water, Mater. Chem. Phys. 239 (2020) 122028, https://doi.org/10.1016/j.matchemphys.2019.122028.
[67] C. Bai, L. Wang, Z. Zhu, Adsorption of Cr(III) and Pb(II) by graphene oxide/alginate hydrogel membrane: Characterization, adsorption kinetics, isotherm and thermodynamics studies, Int. J. Biol. Macromol. 147 (2020) 898–910, https://doi.org/10.1016/j.ijbiomac.2019.09.249.
[68] D. Elhamifar, F. Shojaeipoor, O. Yari, Thiopropyl-containing ionic liquid based periodic mesoporous organosilica as a novel and efficient adsorbent for the removal of Hg(ii) and Pb(ii) ions from aqueous solutions, RSC Adv. 6 (2016) 58658–58666, https://doi.org/10.1039/c6ra08523g.